Available online at www.sciencedirect.com
SCIENCE DIRECT®
Journal of Computational Physics 212 (2006) 490–526
JOURNAL OF COMPUTATIONAL PHYSICS
www.elsevier.com/locate/jcp

The Riemann problem and a high-resolution Godunov method for a model of compressible two-phase flow

D.W. Schwendeman *,[1], C.W. Wahle [2], A.K. Kapila [1]

Department of Mathematical Sciences, Rensselaer Polytechnic Institute, 110 8th Street, Troy, NY 12180, United States

Received 9 December 2004; received in revised form 29 June 2005; accepted 12 July 2005
Available online 1 September 2005

Abstract

This paper considers the Riemann problem and an associated Godunov method for a model of compressible two-phase flow. The model is a reduced form of the well-known Baer–Nunziato model that describes the behavior of granular explosives. In the analysis presented here, we omit source terms representing the exchange of mass, momentum and energy between the phases due to compaction, drag, heat transfer and chemical reaction, but retain the non-conservative nozzling terms that appear naturally in the model. For the Riemann problem the effect of the nozzling terms is confined to the contact discontinuity of the solid phase. Treating the solid contact as a layer of vanishingly small thickness within which the solution is smooth yields jump conditions that connect the states across the contact, as well as a prescription that allows the contribution of the nozzling terms to be computed unambiguously. An iterative method of solution is described for the Riemann problem, that determines the wave structure and the intermediate states of the flow, for given left and right states. A Godunov method based on the solution of the Riemann problem is constructed. It includes non-conservative flux contributions derived from an integral of the nozzling terms over a grid cell. The Godunov method is extended to second-order accuracy using a method of slope limiting, and an adaptive Riemann solver is described and used for computational efficiency. Numerical results are presented, demonstrating the accuracy of the numerical method and in particular, the accurate numerical description of the flow in the vicinity of a solid contact where phases couple and nozzling terms are important. The numerical method is compared with other methods available in the literature and found to give more accurate results for the problems considered.

Keywords: Multiphase flow; Hyperbolic PDEs; Riemann problems; Godunov methods; Shock waves

* Corresponding author. Tel.: +1 518 276 2647; fax: +1 518 276 4824.
E-mail address: schwed@rpi.edu (D.W. Schwendeman).
[1] Research support was given by NSF under Grant DMS-0312040.
[2] Post-doctoral research support was given by NSF under VIGRE Grant DMS-9983646.

0021-9991/$ - see front matter © 2005 Elsevier Inc. All rights reserved.
doi:10.1016/j.jcp.2005.07.012

1. Introduction

This paper considers the Riemann problem and an associated high-resolution Godunov method for a system of nonlinear, hyperbolic partial differential equations modeling compressible, two-phase flow. While models of this kind arise in a number of applications, the context of deflagration-to-detonation transition in high-energy condensed-phase explosives provides the motivation for the present effort. A two-phase continuum description of granular explosives has been provided by Baer and Nunziato [1]; also see the contemporaneous study of Butler and Krier [2], the earlier work of Gokhale and Krier [3], and the later papers of Powers et al. [4,5]. The model treats the explosive as a mixture of two phases, the unreacted granular solid and the gaseous product of combustion. Each phase is assigned a set of state variables such as density, velocity, pressure, etc., which are assumed to satisfy balance laws of mass, momentum and energy. A compaction equation and a saturation constraint for the volume fractions of the phases complete the system of equations. The balance laws for each phase are similar to those for an isolated gas, i.e., the Euler equations, except for two important differences. First, the exchange of mass, momentum and energy between the phases appears as source terms in the balance equations. Second, the governing equations, although hyperbolic, are incapable of being cast in a conservative form. Non-conservative terms (also called *nozzling terms* by analogy with similar terms arising in equations that govern flow within a variable-area duct) appear in the equations, and their treatment requires special consideration.

The aim of this paper is twofold. First, we consider the Riemann problem for the homogeneous portion of the governing equations (i.e., with the source terms omitted), and describe an iterative procedure that produces exact solutions for general left and right states of the initial flow. In the Riemann problem the effect of the nozzling terms is confined to the contact discontinuity of the solid phase, across which the volume fraction of each phase changes discontinuously. It is assumed that the discontinuity can be replaced by a layer of finite but vanishingly small thickness within which the volume fractions vary smoothly and the phases interact. This regularization was first proposed in the context of permeation through a porous solid by Asay et al. [6]. An analysis of the layer yields jump conditions for the states of the flow across the solid contact, and allows the contribution of the nozzling terms to be computed in a straightforward and unambiguous fashion. Away from the solid contact the volume fractions are constant so that balance equations for the phases decouple and reduce to Euler equations for the individual phases. In these regions the usual jump conditions across shocks, rarefactions and the gas contact discontinuity apply, and may be used together with the conditions across the solid contact where the phases are coupled to construct an exact solution of the Riemann problem for the mixture.

Next, the solution of the Riemann problem is employed in the development of a high-resolution Godunov-type method [7]. In addition to providing a means to compute a numerical flux at the boundary between neighboring grid cells, the solution of the Riemann problem provides a natural approach to the numerical treatment of the non-conservative terms. The governing equations are integrated over a grid cell. The numerical flux at the boundary emerges from this integral in the standard way following the usual Godunov flux construction. In the case of the non-conservative terms, the integral reduces to a contribution about the solid contact in the solution of the Riemann problem from each cell boundary. With the thin layer structure of the contact discontinuity at hand, this contribution can be computed unambiguously. Thus the resulting numerical method incorporates both the wave structure at cell boundaries and the appropriate behavior of the solution near the solid contact.

A high-resolution method is obtained using a second-order, slope-limited extension of the Godunov method. The approach follows the usual description (see [8,9], for example) except for the treatment of the non-conservative terms which is new. Essentially, the extension for the non-conservative terms involves two parts, one coming from a contribution to the integral of the nozzling terms about the solid contact and the other coming from the integral away from the jump at the solid contact, which arises from the slope correction of the left and right states of the Riemann problems. An improvement in efficiency in the

numerical method is made by employing various levels of approximation in the solution of the Riemann problem. Here, we describe an adaptive Riemann solver designed to select a suitable approximation, or perhaps the full solution, in order to achieve a sufficient accuracy at a lower computational cost.

Since its introduction, the theory of Baer and Nunziato [1] has received considerable attention in the literature. A mathematical analysis of the structure of the governing equations, including a description of the wave fields of the hyperbolic system, its Riemann invariants and simple wave solutions, was described by Embid and Baer [10]. In this paper, a degeneracy of the hyperbolic system, which occurs when the relative flow between phases becomes sonic, is identified. The authors observe that this degeneracy is analogous to choked flow in a duct, and provides a constraint on the admissible states for the Riemann problem. Modeling issues, certain physically motivated reductions and numerical solutions were presented in a series of papers by Bdzil et al. [11–13]. These papers built upon an analysis of a simpler approach described earlier by Bdzil and Son [14] and Asay et al. [6]. In a recent paper [15], Andrianov and Warnecke revisited the Riemann problem for the model. Using jump conditions across the solid contact, derived in [10], they explicitly constructed *inverse* exact solutions corresponding to prescribed states on either side of the solid contact. Our approach is similar to theirs but differs in one important respect: we describe an iterative procedure to obtain exact solutions of the Riemann problem *directly* for arbitrary left and right states. Such a procedure is necessary as a building block for our construction of a high-resolution Godunov scheme as indicated above and described in detail later.

The regularization of the solid contact into a thin layer across which the solution is smooth no longer applies when the sonic condition is met, i.e., when the gas velocity relative to the solid phase equals the sound speed in the gas. The governing equations exhibit a degeneracy in this case that requires a modified treatment, and this situation is currently under study. However, such a circumstance is unlikely to arise in the context of granular explosives, the application that motivates this study, and is therefore not of concern here. In this application the drag between the phases is invariably large, and serves to keep the relative velocity between the phases at a moderate level so that the system remains subsonic. Consequently, the present study emphasizes the subsonic case.

Finite volume methods for the model equations, or similar forms, have been considered by Gonthier and Powers [16,17], Saurel and Abgrall [18], Andrianov et al. [19], Saurel and Lemetayer [20], Gavrilyuk and Saurel [21] and by Abgrall and Saurel [22], among others. Gonthier and Powers, for example, develop a Godunov-type method for a two-phase flow model and use it to compute solutions to a number of reactive flow problems. Their model equations, however, omit the non-conservative nozzling terms as a modeling choice. As a result, their scheme handles a conservative system with non-differential source terms and thus may be regarded as a straightforward extension of Godunov's method for the Euler equations. The work by Saurel and co-workers considers two-phase models with non-conservative terms. In [18,19], for example, they introduce discrete approximations for the nozzling terms according to a "free-streaming" condition. The basic idea, which is a generalization of the condition given by Abgrall [23], is that a numerical approximation of a two-phase flow with uniform velocity and pressure should maintain uniform velocity and pressure for all time. The high-resolution scheme developed here, based either on the solution of the Riemann problem or an approximation thereof, satisfies this free-streaming condition naturally. It is also shown that the present method provides better agreement near the solid contact layer than methods based on the free-streaming conditions for several test problems.

The remaining sections of the paper are organized as follows. We introduce the model and briefly describe its characteristic framework in Section 2. The Riemann problem is discussed in Section 3. There we describe a thin-layer analysis of the model equations which applies near the solid contact, and describe a two-stage iterative procedure that may be used to obtain exact solutions of the Riemann problem. We consider problems in which the left and right states of the flow consist of a mixture of the phases, as well as problems in which one of the phases vanishes in one of the initial states. Our basic first-order Godunov method is described in Section 4, followed by a discussion of an adaptive Riemann solver in Section 5. A

high-resolution, second-order extension of the basic Godunov method is presented in Section 6, and numerical results for both the first-order and second-order methods are given in Section 7. There we compute numerical solutions of Riemann problems for both the mixture and vanishing phase cases, and we compare solutions given by the present Godunov method with numerical methods suggested by the work in [18,19]. Concluding remarks are made in Section 8.

2. The Governing equations

Assuming one-dimensional flow, the governing equations of the two-phase model, without exchange terms, may be written in the form

$$\mathbf{u}_t + \mathbf{f}_x(\mathbf{u}) = \mathbf{h}(\mathbf{u})\bar{\alpha}_x, \tag{1}$$

where

$$\mathbf{u} = \begin{bmatrix} \bar{\alpha} \\ \bar{\alpha}\bar{\rho} \\ \bar{\alpha}\bar{\rho}\bar{v} \\ \bar{\alpha}\bar{\rho}\bar{E} \\ \alpha\rho \\ \alpha\rho v \\ \alpha\rho E \end{bmatrix}, \quad \mathbf{f}(\mathbf{u}) = \begin{bmatrix} 0 \\ \bar{\alpha}\bar{\rho}\bar{v} \\ \bar{\alpha}(\bar{\rho}\bar{v}^2 + \bar{p}) \\ \bar{\alpha}\bar{v}(\bar{\rho}\bar{E} + \bar{p}) \\ \alpha\rho v \\ \alpha(\rho v^2 + p) \\ \alpha v(\rho E + p) \end{bmatrix}, \quad \mathbf{h}(\mathbf{u}) = \begin{bmatrix} -\bar{v} \\ 0 \\ +p \\ +p\bar{v} \\ 0 \\ -p \\ -p\bar{v} \end{bmatrix}.$$

Here, α, ρ, v and p denote the volume fraction, density, velocity and pressure of the gas phase, respectively, and $\bar{\alpha}$, $\bar{\rho}$, $\bar{v}$ and $\bar{p}$ denote the analogous quantities of the solid phase. (The bar superscript will be used throughout the paper to indicate solid phase quantities.) The total energies are given by

$$E = e + \frac{1}{2}v^2, \quad \bar{E} = \bar{e} + \frac{1}{2}\bar{v}^2,$$

where $e = e(\rho, p)$ and $\bar{e} = \bar{e}(\bar{\rho}, \bar{p})$ are internal energies of the gas and solid, respectively, assuming some equations of state. Finally, the volume fractions satisfy the saturation constraint,

$$\alpha + \bar{\alpha} = 1,$$

which closes the system of equations.

The governing equations in (1) involve both conservative and non-conservative terms. The conservative terms are included in the flux $\mathbf{f}(\mathbf{u})$, which is similar to the flux terms in the Euler equations for a single-phase flow. The non-conservative terms appear on the right-hand side of (1). These terms appeared in Baer and Nunziato's original derivation and additional arguments justifying their presence were given in [12]. They are often referred to as nozzling terms, as noted previously, since they are similar to the terms that appear in the one-dimensional (hydraulic) formulation of flow in a channel with variable cross-sectional area. Here, the volume fraction of the solid plays the role of the area $A(x)$ of the channel. If $\bar{\alpha}_x > 0$, then the flow of the gas sees a converging channel, whereas if $\bar{\alpha}_x < 0$, then the channel diverges.

The governing equations are hyperbolic, but not strictly hyperbolic as discussed in [10]. The seven real eigenvalues are

$$\lambda_1 = \bar{v} - \bar{a}, \quad \lambda_2 = \lambda_3 = \bar{v}, \quad \lambda_4 = \bar{v} + \bar{a}, \quad \lambda_5 = v - a, \quad \lambda_6 = v, \quad \lambda_7 = v + a,$$

where a and $\bar{a}$ are the sound speeds for the gas and solid, respectively. The C_- and C_+ characteristics for each phase given by (λ_1, λ_5) and (λ_4, λ_7), respectively, are genuinely nonlinear, while the characteristics given

by $(\lambda_2, \lambda_3, \lambda_6)$ which represent particle paths of the solid and gas phases are linearly degenerate. The eigenvectors associated with these seven eigenvalues are linearly independent provided that

$$\bar{\alpha} \neq 0, \quad \alpha \neq 0, \quad (v - \bar{v})^2 \neq a^2.$$

The first two conditions are met if the flow is a mixture of both phases, while the last condition is met if the $C_\pm$ characteristics of the gas do not coincide with the particle paths of the solid. Following [10], we shall refer to the latter constraint as the *sonic* condition, as it corresponds to choked flow in a one-dimensional channel. Violating the sonic condition leads to a parabolic degeneracy as discussed in [10,15]. High drag between the phases in the granular-explosives context makes the "subsonic" case,

$$(v - \bar{v})^2 < a^2, \tag{2}$$

more relevant. We consider this case in detail in our analysis and numerical method, but provide a brief description of the supersonic case for completeness. We usually assume a mixture so that $\bar{\alpha} \neq 0$ and $\alpha \neq 0$, but special cases in which one of the phases vanishes in the flow will also be treated.

3. The Riemann problem

The Riemann problem for the two-phase model is

$$\mathbf{u}_t + \mathbf{f}_x(\mathbf{u}) = \mathbf{h}(\mathbf{u})\bar{\alpha}_x, \quad |x| < \infty, \ \ t > 0, \tag{3}$$

with initial conditions

$$\mathbf{u}(x,0) = \begin{cases} \mathbf{u}_\mathrm{L} & \text{if } x < 0, \\ \mathbf{u}_\mathrm{R} & \text{if } x > 0, \end{cases}$$

where $\mathbf{u}_\mathrm{L}$ and $\mathbf{u}_\mathrm{R}$ are given left and right states of the flow. The general structure of the solution, as discussed in [15], consists of shocks and/or rarefactions in the $C_\pm$ characteristic fields, and contact discontinuities along particle paths. For example, the solution shown in Fig. 1 has shocks in the C_- characteristic field of the gas phase and the C_+ characteristic field of solid phase, and has rarefactions in the C_- characteristic field of the solid phase and the C_+ characteristic field of the gas phase. The volume fractions of the solid and gas remain constant to the left and right of the contact discontinuity in the solid phase as indicated in the figure. In these regions of constant $\bar{\alpha}$, the governing equations reduce to Euler equations for the solid and gas phase variables separately. The coupling between phases, and where the nozzling terms play a role, is confined to a vanishing thin region about the solid contact, which we discuss in Section 3.1.

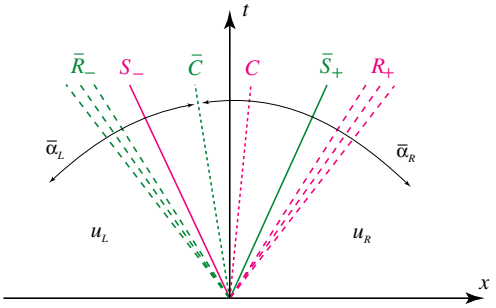

Fig. 1. A representative solution of the Riemann problem consisting of shocks, rarefactions and contact discontinuities indicated by the symbols S, R and C, respectively. (Bar superscripts refer to solid phase quantities.)

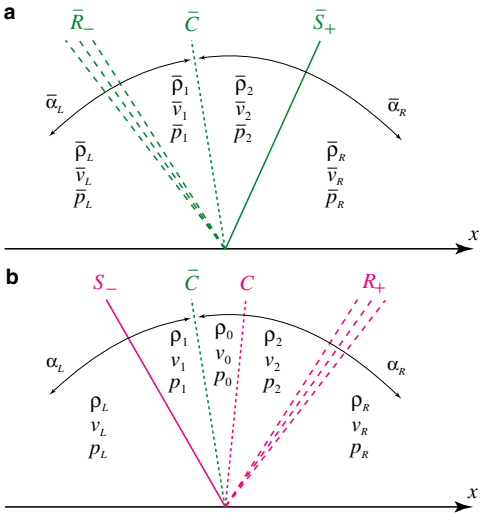

Fig. 2. Intermediate states of the (a) solid and (b) gas phases for a subsonic solid contact.

The intermediate states of the solid and gas phases are indicated in Figs. 2(a) and (b), respectively. For the solid phase, we denote the states to the left and right of the solid contact with subscripts 1 and 2, respectively. A similar notation is used for the intermediate states of the gas, but with an additional intermediate state appearing between the solid and gas contacts. This additional state is given subscript 0, and we note that $v_0 = v_2$ and $p_0 = p_2$ for the configuration shown since the velocity and pressure are continuous across the gas contact (where α and $\bar{\alpha}$ are constant and the contact behaves as a usual contact discontinuity for the Euler equations).

Even though the solution structure of the solid phase (as shown in Fig. 2(a)) is similar to that of the usual Euler equations, it is important to note that the intermediate states of the solid are coupled to those of the gas in accordance with the solid contact jump conditions as discussed below. Thus, the solution for the solid phase cannot be determined independently of the gas phase in general.

For the present discussion, we assume that neither phase vanishes in the flow and that the subsonic condition in (2) is met. The latter condition implies that the solid contact lies between the shocks/rarefactions of the gas as is the case shown in Fig. 2(b). The gas contact, on the other hand, may lie to the left or to the right of the solid contact, or it may lie on either side of the shocks/rarefactions of the solid. Fig. 2(b) shows the solid contact to the left of the gas contact. If the positions are reversed, then $v_0 = v_1$ and $p_0 = p_1$ according to the continuity of velocity and pressure across the gas contact as mentioned above.

On either side of the solid contact where $\bar{\alpha}$ is constant, the equations reduce to a pair of Euler equations for each phase separately. Accordingly, the jump conditions across shocks and rarefactions are the same as those for the Euler equations with the chosen equation of state. Following the discussion in [24], we choose to parameterize the states across shocks/rarefactions with pressure, and set

$$v_1 = v_{\mathrm{L}} - F_{\mathrm{L}}(p_1), \quad \rho_1 = G_{\mathrm{L}}(p_1), \quad \bar{v}_1 = \bar{v}_{\mathrm{L}} - \bar{F}_{\mathrm{L}}(\bar{p}_1), \quad \bar{\rho}_1 = \bar{G}_{\mathrm{L}}(\bar{p}_1), \tag{4}$$

in region 1, and

$$v_2 = v_{\mathrm{R}} + F_{\mathrm{R}}(p_2), \quad \rho_2 = G_{\mathrm{R}}(p_2), \quad \bar{v}_2 = \bar{v}_{\mathrm{R}} + \bar{F}_{\mathrm{R}}(\bar{p}_2), \quad \bar{\rho}_2 = \bar{G}_{\mathrm{R}}(\bar{p}_2), \tag{5}$$

in region 2. For an ideal gas with polytropic exponent γ, the functions $F_s(p)$ and $G_s(p)$, $s = \mathrm{L}$ or R, are given by

$$F_s(p) = \begin{cases} (p - p_s)\left[\frac{A_s}{p+B_s}\right]^{1/2} & \text{if } p > p_s \text{ (shock)}, \\ \frac{2a_s}{(\gamma-1)}\left[\left(\frac{p}{p_s}\right)^{(\gamma-1)/2\gamma} - 1\right] & \text{if } p < p_s \text{ (rarefaction)}, \end{cases} \tag{6}$$

and

$$G_s(p) = \begin{cases} \rho_s\left[\frac{(\gamma-1)p_s+(\gamma+1)p}{(\gamma-1)p+(\gamma+1)p_s}\right] & \text{if } p > p_s \text{ (shock)}, \\ \rho_s\left(\frac{p}{p_s}\right)^{1/\gamma} & \text{if } p < p_s \text{ (rarefaction)}, \end{cases} \tag{7}$$

where

$$A_s = \frac{2}{(\gamma+1)\rho_s}, \quad B_s = \frac{(\gamma-1)}{(\gamma+1)}p_s, \quad a_s = \sqrt{\frac{\gamma p_s}{\rho_s}}. \tag{8}$$

For the solid, we assume a stiffened gas equation of state with polytropic exponent $\bar{\gamma}$ and constant stiffening pressure $\bar{p}_0$. For this choice, $\bar{F}_s(\bar{p})$ and $\bar{G}_s(\bar{p})$, $s = \mathrm{L}$ or R, become

$$\bar{F}_s(\bar{p}) = \begin{cases} (\bar{p} - \bar{p}_s)\left[\frac{\bar{A}_s}{\bar{p}+\bar{p}_0+\bar{B}_s}\right]^{1/2} & \text{if } \bar{p} > \bar{p}_s \text{ (shock)}, \\ \frac{2\bar{a}_s}{(\bar{\gamma}-1)}\left[\left(\frac{\bar{p}+\bar{p}_0}{\bar{p}_s+\bar{p}_0}\right)^{(\bar{\gamma}-1)/2\bar{\gamma}} - 1\right] & \text{if } \bar{p} < \bar{p}_s \text{ (rarefaction)}, \end{cases} \tag{9}$$

and

$$\bar{G}_s(\bar{p}) = \begin{cases} \bar{\rho}_s\left[\frac{(\bar{\gamma}-1)(\bar{p}_s+\bar{p}_0)+(\bar{\gamma}+1)(\bar{p}+\bar{p}_0)}{(\bar{\gamma}-1)(\bar{p}+\bar{p}_0)+(\bar{\gamma}+1)(\bar{p}_s+\bar{p}_0)}\right] & \text{if } \bar{p} > \bar{p}_s \text{ (shock)}, \\ \bar{\rho}_s\left(\frac{\bar{p}+\bar{p}_0}{\bar{p}_s+\bar{p}_0}\right)^{1/\bar{\gamma}} & \text{if } \bar{p} < \bar{p}_s \text{ (rarefaction)}, \end{cases} \tag{10}$$

where

$$\bar{A}_s = \frac{2}{(\bar{\gamma}+1)\bar{\rho}_s}, \quad \bar{B}_s = \frac{(\bar{\gamma}-1)}{(\bar{\gamma}+1)}(\bar{p}_s + \bar{p}_0), \quad \bar{a}_s = \sqrt{\frac{\bar{\gamma}(\bar{p}_s+\bar{p}_0)}{\bar{\rho}_s}}. \tag{11}$$

Similar expressions to those in (6), (7), (9) and (10) may be derived for other equations of state, but the choice of equation of state is not significant for the analysis of the Riemann problem or for the development of the numerical method that follows, and so the functions above are sufficient for the purposes of this paper.

The state of the flow in regions 1 and 2 is determined completely by the pressures (p_1, p_2) of the gas and $(\bar{p}_1, \bar{p}_2)$ of the solid. These pressures also determine whether the transitions are shocks or rarefactions, and they specify the positions of these waves. The density ρ_0 of the gas in region 0 is the remaining unknown. The jump conditions across the solid contact provide the necessary equations to determine these five quantities. An analysis of the solid contact which results in the jump conditions is discussed next, and a method of iteration to solve the equations is presented in Section 3.2.

3.1. Solid contact

We now consider the governing equations in the vicinity of the solid contact. It is here that the nozzling terms play a role and the phases couple in the solution of the Riemann problem. Since the nozzling terms are not conservative, an analysis based upon an integral conservation does not apply here and we turn

instead to a thin-layer analysis similar to that described in [6]. For this analysis, we require two rather mild assumptions, namely, that the layer is vanishingly thin, and that the solution through the layer is smooth. Accordingly, we consider traveling wave solutions of the governing equations in terms of the independent variable $\xi = x - Ut$, which measures scaled distance across the layer traveling with a constant velocity U. In terms of the variable ξ, the model equations become

$$-U\mathbf{u}_\xi + \mathbf{f}_\xi(\mathbf{u}) = \mathbf{h}(\mathbf{u})\bar{\alpha}_\xi. \tag{12}$$

The first component of (12) reads

$$-U\bar{\alpha}_\xi = -\bar{v}\bar{\alpha}_\xi,$$

which implies that $\bar{\alpha}_\xi = 0$ or $U = \bar{v}$. The former case implies $\bar{\alpha} =$ constant across the layer and leads to a decoupling of the equations for the gas and solid as noted previously. Here, we concentrate on the latter case which leads to jump conditions across the solid contact.

With $U = \bar{v}$, the three equations in (12) for the solid become

$$\begin{aligned}
&-\bar{v}(\bar{\alpha}\bar{\rho})_\xi + (\bar{\alpha}\bar{\rho}\bar{v})_\xi = 0,\\
&-\bar{v}(\bar{\alpha}\bar{\rho}\bar{v})_\xi + (\bar{\alpha}\bar{\rho}\bar{v}^2 + \bar{\alpha}\bar{p})_\xi = p\bar{\alpha}_\xi,\\
&-\bar{v}(\bar{\alpha}\bar{\rho}\bar{E})_\xi + (\bar{\alpha}\bar{v}\bar{\rho}\bar{E} + \bar{\alpha}\bar{v}\bar{p})_\xi = p\bar{v}\bar{\alpha}_\xi.
\end{aligned}$$

The first of these three equations is satisfied identically, while the second and third equations both give

$$(\bar{\alpha}\bar{p})_\xi = p\bar{\alpha}_\xi. \tag{13}$$

The three remaining equations in (12) for the gas are

$$-\bar{v}(\alpha\rho)_\xi + (\alpha\rho v)_\xi = 0, \tag{14}$$

$$-\bar{v}(\alpha\rho v)_\xi + (\alpha\rho v^2 + \alpha p)_\xi = -p\bar{\alpha}_\xi, \tag{15}$$

$$-\bar{v}(\alpha\rho E)_\xi + (\alpha v\rho E + \alpha v p)_\xi = -p\bar{v}\bar{\alpha}_\xi. \tag{16}$$

A straightforward manipulation of (13)–(16) leads to a set of jump conditions involving a balance of mass, momentum, enthalpy and entropy across the layer. An equation for the mass flux of the gas across the layer follows immediately from (14), and takes the form

$$\alpha\rho(v - \bar{v}) = K_1, \tag{17}$$

where K_1 is a constant of integration. An equation for momentum may be obtained from (13)–(15), and is given by

$$\alpha\rho(v - \bar{v})^2 + \alpha p + \bar{\alpha}\bar{p} = K_2, \tag{18}$$

where K_2 is another constant of integration. Next, we may use (14)–(16) to obtain

$$\alpha\rho(v - \bar{v})\left[h + \frac{1}{2}(v - \bar{v})^2\right]_\xi = 0, \tag{19}$$

where $h(\rho,p) = e + p/\rho$ is the enthalpy of the gas. If the mass flux across the layer is not zero, then (19) reduces to

$$h + \frac{1}{2}(v - \bar{v})^2 = K_3, \tag{20}$$

where K_3 is a constant. The final jump condition involves the entropy of the gas. Upon manipulation of the original four independent layer equations, we find

$$\bar{\alpha}\rho(v-\bar{v})\left[e_\xi + p\left(\frac{1}{\rho}\right)_\xi\right] = 0,$$

or

$$\bar{\alpha}\rho(v-\bar{v})S_\xi = 0, \tag{21}$$

using the thermodynamic identity $\mathrm{d}e + p\,\mathrm{d}(1/\rho) = T\,\mathrm{d}S$, where $S(\rho,p)$ is the entropy of the gas. As before, if the mass flux across the layer is not zero, then we have $S = K_4 = \text{constant}$ which provides the last jump condition from the four independent layer equations. These four jump conditions, along with the constraint that $\bar{v} = \text{constant}$ across the layer, are the same as those used in [15] following the work in [10], and they provide enough equations to complete the solution of the Riemann problem as we discuss below. The layer equations also provide a useful guide to the numerical treatment of the non-conservative terms in our Godunov method as we discuss in Section 4.

3.2. Iterative solution

For the solution configuration of Fig. 2, the jump conditions at the solid contact imply the equations

$$\begin{aligned}
&\bar{v}_1 = \bar{v}_2,\\
&\alpha_{\mathrm{L}}\rho_1(v_1-\bar{v}_1) = \alpha_{\mathrm{R}}\rho_0(v_2-\bar{v}_2),\\
&\bar{\alpha}_{\mathrm{L}}\bar{p}_1 + \alpha_{\mathrm{L}}p_1 + \alpha_{\mathrm{L}}\rho_1(v_1-\bar{v}_1)^2 = \bar{\alpha}_{\mathrm{R}}\bar{p}_2 + \alpha_{\mathrm{R}}p_2 + \alpha_{\mathrm{R}}\rho_0(v_2-\bar{v}_2)^2,\\
&\frac{\gamma p_1}{(\gamma-1)\rho_1} + \frac{1}{2}(v_1-\bar{v}_1)^2 = \frac{\gamma p_2}{(\gamma-1)\rho_0} + \frac{1}{2}(v_2-\bar{v}_2)^2,\\
&\frac{p_1}{\rho_1^\gamma} = \frac{p_2}{\rho_0^\gamma},
\end{aligned}$$

assuming an ideal gas. Recalling the relations in (4) and (5), we may regard these jump conditions as five equations for the unknowns $(\rho_0, p_1, p_2, \bar{p}_1, \bar{p}_2)$, or, preferably, we may eliminate ρ_0 from the equations using the entropy equation, and then view the remaining four equations as a system of nonlinear algebraic equations for the four pressures. These equations have the vector form

$$\mathbf{N}(p_1, p_2, \bar{p}_1, \bar{p}_2) = 0, \tag{22}$$

where the four components of $\mathbf{N}$ may be taken as

$$\begin{aligned}
N_1 &= \bar{v}_2 - \bar{v}_1,\\
N_2 &= \alpha_{\mathrm{R}}\left(\frac{p_2}{p_1}\right)^{1/\gamma}(v_2-\bar{v}_2) - \alpha_{\mathrm{L}}(v_1-\bar{v}_1),\\
N_3 &= \bar{\alpha}_{\mathrm{R}}\bar{p}_2 + \alpha_{\mathrm{R}}p_2 - \bar{\alpha}_{\mathrm{L}}\bar{p}_1 - \alpha_{\mathrm{L}}p_1 + \alpha_{\mathrm{L}}\rho_1(v_1-\bar{v}_1)(v_2-v_1),\\
N_4 &= \frac{\gamma p_2}{(\gamma-1)\rho_1}\left(\frac{p_1}{p_2}\right)^{1/\gamma} + \frac{1}{2}(v_2-\bar{v}_2)^2 - \frac{\gamma p_1}{(\gamma-1)\rho_1} - \frac{1}{2}(v_1-\bar{v}_1)^2.
\end{aligned} \tag{23}$$

The nonlinear algebraic system (22) with components (23) may be solved iteratively for given left and right states using Newton's method. The iteration requires starting values $(p_1^{(0)}, p_2^{(0)}, \bar{p}_1^{(0)}, \bar{p}_2^{(0)})$ for the pressures of the intermediate states. We use

$$p_1^{(0)} = p_2^{(0)} = p_*, \quad \bar{p}_1^{(0)} = \bar{p}_2^{(0)} = \bar{p}_*,$$

where p_*, $\bar{p}_*$ are defined implicitly by the equations

$$v_* = v_L - F_L(p_*) = v_R + F_R(p_*), \quad \bar{v}_* = \bar{v}_L - \bar{F}_L(\bar{p}_*) = \bar{v}_R + \bar{F}_R(\bar{p}_*), \tag{24}$$

respectively. These "star" values correspond to the velocities and pressures for the gas and solid in the intermediate states assuming a decoupled flow in which $\bar{\alpha} = \text{constant}$. Thus, this choice of starting values for Newton's method is particularly relevant for the case when the difference between $\bar{\alpha}_R$ and $\bar{\alpha}_L$ is small, which often occurs if the left and right states are given by neighboring grid cells in a Godunov-type scheme (see Section 4). However, our numerical experiments have shown that this choice is suitable even when the difference in the volume fractions is not small as we show in a representative Riemann problem below.

Our iterative scheme proceeds in two stages. The first stage involves two independent Newton iterations to obtain p_* and $\bar{p}_*$ approximately. These iterations are equivalent to finding the solutions of the Riemann problem for the Euler equations for each phase separately (see [24] for a detailed discussion of this iteration). The second stage involves a Newton iteration to solve the solid contact jump conditions for the coupled problem assuming $\bar{\alpha}_L \neq \bar{\alpha}_R$. If $v_* > \bar{v}_*$ as determined by the solution of the first stage, then we initially assume the configuration shown in Fig. 2 for the second stage and solve (22) with components given by (23) for the intermediate pressures $(p_1, p_2, \bar{p}_1, \bar{p}_2)$. If, on the other hand, $v_* < \bar{v}_*$, then we first assume that the gas contact lies to the left of the solid contact and consider the iterative solution of (22) but with components

$$\begin{aligned}
N_1 &= \bar{v}_2 - \bar{v}_1, \\
N_2 &= \alpha_R(v_2 - \bar{v}_2) - \alpha_L\left(\frac{p_1}{p_2}\right)^{1/\gamma}(v_1 - \bar{v}_1), \\
N_3 &= \bar{\alpha}_R\bar{p}_2 + \alpha_R p_2 - \bar{\alpha}_L\bar{p}_1 - \alpha_L p_1 + \alpha_R\rho_2(v_2 - \bar{v}_2)(v_2 - v_1), \\
N_4 &= \frac{\gamma p_2}{(\gamma-1)\rho_2} + \frac{1}{2}(v_2 - \bar{v}_2)^2 - \frac{\gamma p_1}{(\gamma-1)\rho_2}\left(\frac{p_2}{p_1}\right)^{1/\gamma} - \frac{1}{2}(v_1 - \bar{v}_1)^2,
\end{aligned} \tag{25}$$

suitable for this solution configuration. During the subsequent steps of the Newton iteration the sign of $v_1 - \bar{v}_1$ is checked to determine which set of equations is appropriate.

As an example, consider the Riemann problem with left and right states given in Table 1. In this example, the initial two-phase mixture is at rest with a decrease in the volume fraction of the solid at $x = 0$ initially from $\bar{\alpha}_L = 0.8$ to $\bar{\alpha}_R = 0.3$. The solid density and pressure are equal on either side of $x = 0$ at $t = 0$. The gas pressure is high on the right which drives a shock wave in the gas towards the left with $x/t = -1.982$ and a rarefaction towards the right for $1.044 \leqslant x/t \leqslant 1.183$. The response of the solid is a shock wave moving to the right with $x/t = 1.225$ and a rarefaction moving to left for $-1.183 \leqslant x/t \leqslant -1.101$. The intermediate states of the flow are computed using our iterative procedure and are included in Table 1. An x–t diagram for each phase and the solution at $t = 0.2$ is shown in Fig. 3.

The solution of the Riemann problem shown in Fig. 3 involves one of many possible combinations of shocks and/or rarefactions in the solid and gas phases. Our two-stage iterative procedure makes no initial assumption of the solution structure, but rather determines it as part of the process. The only essential

Table 1
Left and right states and the computed intermediate states for a sample Riemann problem with $\gamma = \bar{\gamma} = 1.4$ and $\bar{p}_0 = 0$

	Region L	Region 1	Region 0	Region 2	Region R
$\bar{\alpha}$	0.8	0.8	0.8	0.3	0.3
$\bar{\rho}$	1.0	0.9436	0.9436	1.0591	1.0
$\bar{v}$	0.0	0.0684	0.0684	0.0684	0.0
$\bar{p}$	1.0	0.9219	0.9219	1.0837	1.0
ρ	0.2	0.3266	0.6980	0.9058	1.0
v	0.0	−0.7683	−0.7683	−0.1159	0.0
p	0.3	0.6045	0.6045	0.8707	1.0

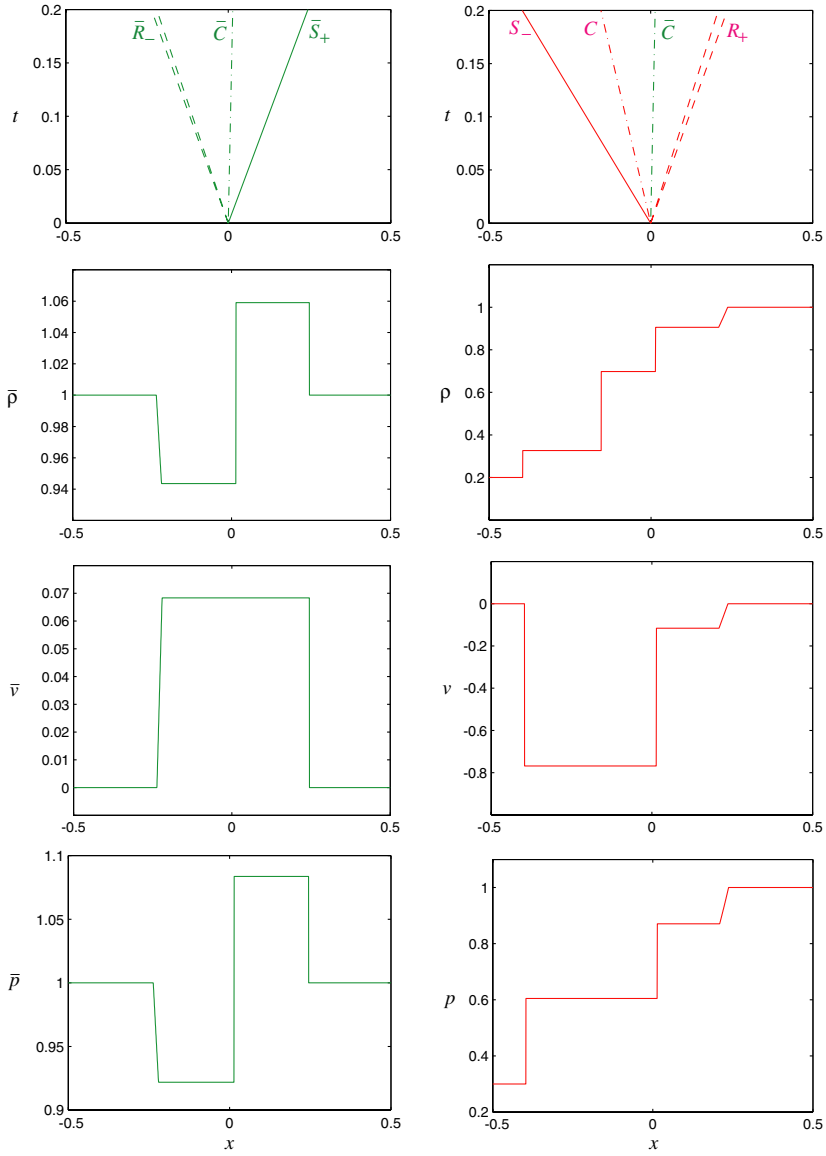

Fig. 3. Solution of the Riemann problem for the left and right states given in Table 1. The solid variables appear in the plots on the left and the gas variables appear on the right.

restriction is that the sonic condition is met. Assuming that the sonic condition is satisfied, it can be shown (see Section 5.2) that the solution of the solid contact jump conditions, and thus the solution of the Riemann problem, is unique for flows in which $|\bar{\alpha}_R - \bar{\alpha}_L|$ is sufficiently small. This branch of solutions may be followed for Riemann problems in which $|\bar{\alpha}_R - \bar{\alpha}_L|$ increases (holding the other quantities in the left and right states fixed) until $|\bar{\alpha}_R - \bar{\alpha}_L| = 1$ or until the sonic condition is violated at which point solutions cease to exist according to the analysis given in [15]. Thus, for a given left and right states, we regard the unique solution of the Riemann problem to be the one that satisfies the solid contact jump conditions

(along the branch of solutions described) and satisfies the usual (entropy-satisfying) jump conditions at shocks, rarefactions and the gas contact discontinuity away from the solid contact.

3.3. Vanishing phase cases

An exact solution of the Riemann problem may be constructed for the special cases in which the solid or the gas phase vanishes in one of the initial states. For these cases, the solid contact separates the mixture from the single phase region. Thus, we need to revisit the thin-layer equations for the solid contact for the vanishing phase cases to sort out the appropriate structure of the solution and the corresponding jump conditions required to determine it.

For example, consider the case in which $0 < \bar{\alpha}_L < 1$ and $\bar{\alpha}_R = 0$ as shown in Fig. 4 so that the left state is a mixture while the right state consists of only the gas phase. Here, we need only specify the solid primitive variables $(\bar{\rho}_L, \bar{v}_L, \bar{p}_L)$ in the left state, as shown in the figure, whereas we need to supply both the left and right primitive states for the gas. The solution for the solid phase involves a shock or rarefaction in the C_- characteristic field (e.g., a rarefaction is shown) and an intermediate state with subscript 1 to the left of the solid contact. The structure of the solution for the gas phase remains the same as that shown in Fig. 2(b), although the contact discontinuity of the gas may lie on either side of the solid contact (and shocks may be replaced by rarefactions and vice versa). If the contact discontinuity of the gas lies to the right of the solid contact, then the jump conditions at the solid contact become

$$\begin{aligned}
&\alpha_L \rho_1 (v_1 - \bar{v}_1) = \rho_0 (v_2 - \bar{v}_1),\\
&\bar{\alpha}_L \bar{p}_1 + \alpha_L p_1 + \alpha_L \rho_1 (v_1 - \bar{v}_1)^2 = p_2 + \rho_0 (v_2 - \bar{v}_1)^2,\\
&\frac{\gamma p_1}{(\gamma - 1)\rho_1} + \frac{1}{2}(v_1 - \bar{v}_1)^2 = \frac{\gamma p_2}{(\gamma - 1)\rho_0} + \frac{1}{2}(v_2 - \bar{v}_1)^2,\\
&\frac{p_1}{\rho_1^\gamma} = \frac{p_2}{\rho_0^\gamma}.
\end{aligned}$$

These jump conditions determine the values for $(\rho_0, p_1, p_2, \bar{p}_1)$, or simply $(p_1, p_2, \bar{p}_1)$ if the entropy equation is used to eliminate ρ_0 as before.

We use a slight variation of the two-stage iterative procedure described earlier to solve the jump conditions for $(p_1, p_2, \bar{p}_1)$. The first stage uses Newton's method to compute p_* and v_* for the gas as before. We then set $\bar{p}_* = p_*$ and $\bar{v}_* = \bar{v}_L - \bar{F}_L(\bar{p}_*)$ for the solid, and apply Newton's method to the three equations for the jump conditions at the solid contact. These equations have the form

$$\tilde{\mathbf{N}}(p_1, p_2, \bar{p}_1) = 0, \tag{26}$$

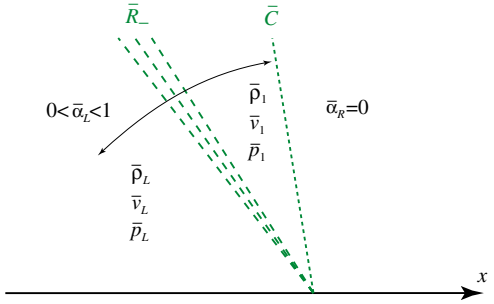

Fig. 4. A vanishing solid case in which the left state is a mixture while the right state consists of only the gas phase. (The C_- characteristic field may be a rarefaction as shown or a shock.)

with components

$$\tilde{N}_1 = \left(\frac{p_2}{p_1}\right)^{1/\gamma}(v_2 - \bar{v}_1) - \alpha_L(v_1 - \bar{v}_1),$$
$$\tilde{N}_2 = p_2 - \bar{\alpha}_L\bar{p}_1 - \alpha_L p_1 + \alpha_L\rho_1(v_1 - \bar{v}_1)(v_2 - v_1),$$
$$\tilde{N}_3 = \frac{\gamma p_2}{(\gamma-1)\rho_1}\left(\frac{p_1}{p_2}\right)^{1/\gamma} + \frac{1}{2}(v_2 - \bar{v}_1)^2 - \frac{\gamma p_1}{(\gamma-1)\rho_1} - \frac{1}{2}(v_1 - \bar{v}_1)^2,$$

if $v_* > \bar{v}_*$, or with components

$$\tilde{N}_1 = (v_2 - \bar{v}_1) - \alpha_L\left(\frac{p_1}{p_2}\right)^{1/\gamma}(v_1 - \bar{v}_1),$$
$$\tilde{N}_2 = p_2 - \bar{\alpha}_L\bar{p}_1 - \alpha_L p_1 + \alpha_R\rho_2(v_2 - \bar{v}_1)(v_2 - v_1),$$
$$\tilde{N}_3 = \frac{\gamma p_2}{(\gamma-1)\rho_2} + \frac{1}{2}(v_2 - \bar{v}_1)^2 - \frac{\gamma p_1}{(\gamma-1)\rho_2}\left(\frac{p_2}{p_1}\right)^{1/\gamma} - \frac{1}{2}(v_1 - \bar{v}_1)^2,$$

otherwise. Similar equations apply if the left and right states are reversed so that the solid phase vanishes in the left state.

Fig. 5 shows the solution of a Riemann problem representative of the case when the solid phase vanishes in the right initial state. The values for the left and right states are given in Table 2 along with the computed values for the intermediate states. For this example, the solution consists of a rarefaction in the C_- characteristic field of the solid phase for $-2.739 \leqslant x/t \leqslant -2.144$ and a solid contact which moves with speed $x/t = 0.297$. The solution for the gas phase consists of a shock for $x/t = -2.058$, a contact discontinuity for $x/t = -0.5824$ and a rarefaction for $1.645 \leqslant x/t \leqslant 1.764$.

The opposite situation occurs when the gas phase vanishes in the left or right states. For example, let us consider the case when $\alpha_L = 0$ and $0 < \alpha_R < 1$ so that there is no gas phase in the left state while the right state is a mixture. Since the gas phase vanishes through the solid contact, it follows that the mass flux of gas across the solid contact is zero. Accordingly, the contact discontinuity for the gas collapses upon that of the solid and region 0 disappears as shown in Fig. 6. There is a shock or rarefaction in the C_+ characteristic field (e.g., a rarefaction is shown) and an intermediate state with subscript 2 to the right of the solid/gas contact. The solution structure for the solid phase remains the same as that shown in Fig. 2(a). Thus, the jump conditions at the solid contact reduce to

$$\widehat{\mathbf{N}}(p_2, \bar{p}_1, \bar{p}_2) = 0, \tag{27}$$

where

$$\widehat{N}_1 = \bar{v}_2 - \bar{v}_1,$$
$$\widehat{N}_2 = \bar{v}_2 - v_2,$$
$$\widehat{N}_3 = \bar{\alpha}_R\bar{p}_2 + \alpha_R p_2 - \bar{p}_1,$$

which determine the pressures $(p_2, \bar{p}_1, \bar{p}_2)$. The jump conditions involving the enthalpy and entropy of the gas do not apply since the mass flux of the gas across the solid contact is zero.

In order to solve (27), we first determine $\bar{p}_*$ and $\bar{v}_*$ using Newton's method as described in Section 3.2, and then determine p_* iteratively from the equation $\bar{v}_* = v_R + F_R(p_*)$. From here, we use $p_2^{(0)} = p_*$ and $\bar{p}_1^{(0)} = \bar{p}_2^{(0)} = \bar{p}_*$ as starting values for a Newton iteration to solve (27). A representative solution is shown in Fig. 7 for the left and right states given in Table 3. Here, we consider a mixture at rest in the right state at $t = 0$ and a solid at rest in the left state. There is a large pressure difference between the left and right

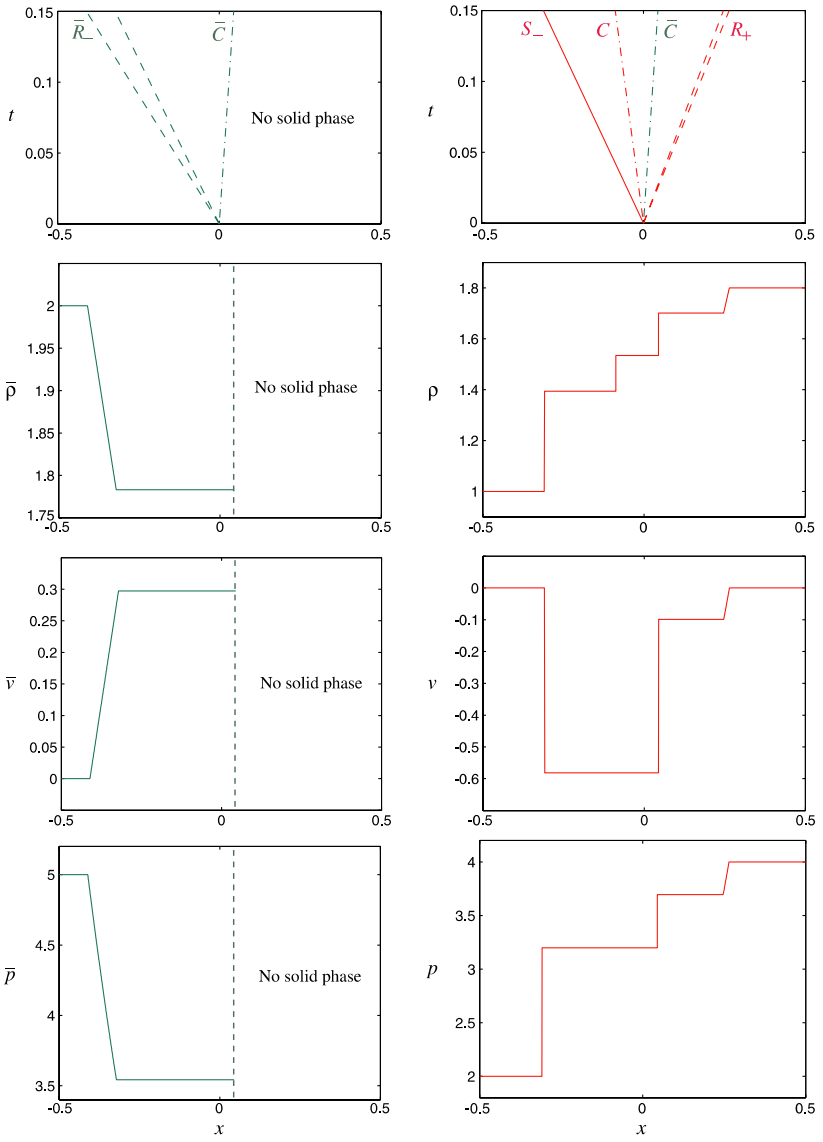

Fig. 5. Solution of the Riemann problem for the left and right states given in Table 2. The solid variables appear in the plots on the left and the gas variables appear on the right. The solid phase vanishes to the right of the solid contact.

states of the solid phase initially which leads to a shock traveling to the right with speed $x/t = 2.336$ and a rarefaction on the left for $-2.739 \leqslant x/t \leqslant -1.816$. The solid contact moves to the right with speed $x/t = 0.461$ which creates a compression in the gas and a shock with speed $x/t = 1.752$.

3.4. Supersonic case

We close our discussion of the exact solution of the Riemann problem by considering briefly the case in which the relative gas velocity is supersonic through the solid contact. In this case, the solid contact lies to

Table 2
Left and right states and the computed intermediate states for a sample Riemann problem with $\gamma = 1.4$, $\bar{\gamma} = 3$ and $\bar{p}_0 = 0$, and for which the right state consists of only the gas phase

	Region L	Region 1	Region 0	Region 2	Region R
$\bar{\alpha}$	0.5	0.5	0.5	0.0	0.0
$\bar{\rho}$	2.0	1.7829	1.7829	–	–
$\bar{v}$	0.0	0.2972	0.2972	–	–
$\bar{p}$	5.0	3.5422	3.5422	–	–
ρ	1.0	1.3941	1.5341	1.7010	1.8
v	0.0	−0.5819	−0.5819	−0.0992	0.0
p	2.0	3.1978	3.1978	3.6956	4.0

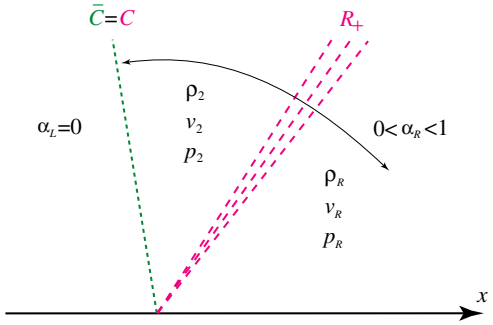

Fig. 6. A vanishing gas case in which the left state consists of only the solid phase while the right state is a mixture. (The C_+ characteristic field may be a rarefaction as shown or a shock.)

one side of all of the characteristic fields of the gas phase. For example, Fig. 8 shows the intermediate states for the solid and gas for a supersonic case in which all of the characteristic fields of the gas lie to the right of the solid contact. As before, the solid pressures $\bar{p}_1$ and $\bar{p}_2$ determine the density and velocity of the solid to the left and right of the solid contact, respectively, so that in this case the jump conditions across the solid contact may be regarded as equations for the states $(\bar{p}_1, \bar{p}_2, \rho_0, v_0, p_0)$. Once these equations are solved (using Newton's method for example), then the remaining intermediate states of the gas in regions 1 and 2 may be found iteratively by considering (ρ_0, v_0, p_0) and (ρ_R, v_R, p_R) as left and right states for a Riemann problem for the gas phase alone. A similar construction occurs when the characteristic fields of the gas lie to the left of the solid contact.

For the reasons mentioned earlier, we are interested primarily in the subsonic case. The supersonic case is described here for completeness, but we will not consider it further. However, it is worth noting that the subsonic case considered previously and the supersonic case discussed here are the only admissible solutions of the Riemann problem in which the solution in the solid contact layer is smooth according to the selection criterion discussed in [15].

4. A Godunov method

We now turn our attention to a description of a Godunov method for the two-phase model. The method requires solutions of the Riemann problem, which we have described in the previous section and now consider to be known. The basic description of our numerical method follows the usual course (see, for

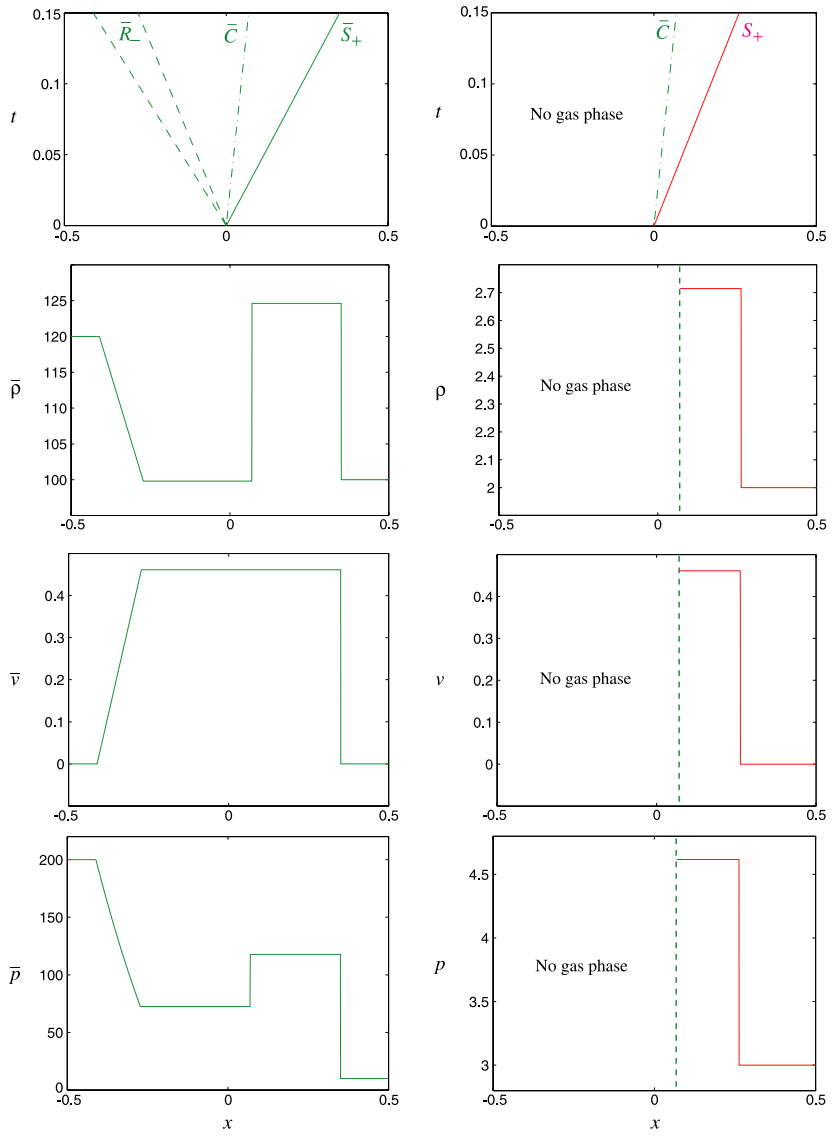

Fig. 7. Solution of the Riemann problem for the left and right states given in Table 3. The solid variables appear in the plots on the left and the gas variables appear on the right. The gas phase vanishes to the left of the solid contact.

example, the discussions in [25] or [24]) except for our numerical treatment of the non-conservative nozzling terms which is new and will be the main focus of our attention. Essentially, the method combines the standard conservative Godunov flux with a non-conservative contribution arising from an integral of the nozzling terms over a grid cell. Both of these contributions are exact for a piecewise constant initial state (and for a sufficiently small time step so that neighboring Riemann problems do not interact). The numerical approximation lies in the piecewise constant interpolation of the solution at each time step, and as a result the numerical method is first-order accurate, but may be extended to second-order accuracy (for smooth regions of the flow) as we describe later in Section 6.

Table 3
Left and right states and the computed intermediate states for a sample Riemann problem with $\gamma = 1.4$, $\bar{\gamma} = 3$ and $\bar{p}_0 = 100$, and for which the left state consists of only the solid phase

	Region L	Region 1	Region 2	Region R
$\bar{\alpha}$	1.0	1.0	0.6	0.6
$\bar{\rho}$	120.0	99.786	124.61	100.0
$\bar{v}$	0.0	0.4613	0.4613	0.0
$\bar{p}$	200.0	72.496	117.75	10.0
ρ	–	–	2.7146	2.0
v	–	–	0.4613	0.0
p	–	–	4.6166	3.0

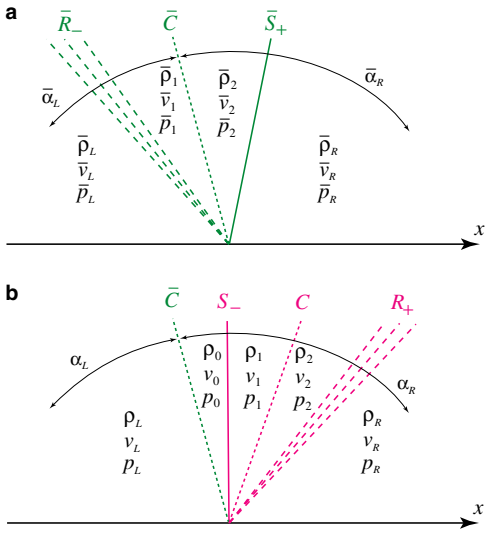

Fig. 8. Intermediate states of the (a) solid and (b) gas phases for a supersonic solid contact.

Let us begin by assuming a uniform grid, $x_j = (j - \frac{1}{2})\Delta x, j = 1, 2, \ldots, N$, with mesh spacing Δx, and define the cell average

$$\mathbf{U}_j^n = \frac{1}{\Delta x} \int_{x_{j-1/2}}^{x_{j+1/2}} \mathbf{u}(x, t_n)\, \mathrm{d}x.$$

An integral of (1) over a grid cell $\Omega_j^n = [x_{j-1/2}, x_{j+1/2}] \times [t_n, t_{n+1}]$ results in the exact formula

$$\mathbf{U}_j^{n+1} = \mathbf{U}_j^n - \frac{\Delta t}{\Delta x}\left(\mathbf{F}_{j+1/2}^n - \mathbf{F}_{j-1/2}^n\right) + \frac{1}{\Delta x}\int\int_{\Omega_j^n} \mathbf{h}(\mathbf{u})\bar{\alpha}_x\, \mathrm{d}x\, \mathrm{d}t, \tag{28}$$

where $\Delta t = t_{n+1} - t_n$ and

$$\mathbf{F}_{j\pm1/2}^n = \frac{1}{\Delta t}\int_{t_n}^{t_{n+1}} \mathbf{f}\left(\mathbf{u}(x_{j\pm1/2}, t)\right) \mathrm{d}t. \tag{29}$$

If we assume a piecewise constant approximation for $\mathbf{u}(x, t)$ at $t = t_n$, i.e.,

$$\mathbf{u}(x,t_n) \approx \begin{cases} \vdots & \\ \mathbf{U}_{j-1}^n & \text{if } x \in [x_{j-3/2}, x_{j-1/2}), \\ \mathbf{U}_j^n & \text{if } x \in [x_{j-1/2}, x_{j+1/2}), \\ \mathbf{U}_{j+1}^n & \text{if } x \in [x_{j+1/2}, x_{j+3/2}), \\ \vdots & \end{cases}$$

then we may evaluate the fluxes $\mathbf{F}^n_{j\pm1/2}$ in (29) and the integral of the nozzling terms in (28) using the solution of the Riemann problem with initial states given by $\mathbf{U}_j^n$ and the corresponding values in the neighboring cells. For example, let $\mathbf{u}^*(\mathbf{u}_L, \mathbf{u}_R)$ be the (constant) value of the self-similar solution of the Riemann problem in (3) along the line $x = 0$ for $t > 0$, and set

$$\mathbf{F}^n_{j-1/2} = \frac{1}{\Delta t}\int_{t_n}^{t_{n+1}} \mathbf{f}\left(\mathbf{u}^*(\mathbf{U}^n_{j-1}, \mathbf{U}^n_j)\right)\,\mathrm{d}t = \mathbf{f}\left(\mathbf{u}^*(\mathbf{U}^n_{j-1}, \mathbf{U}^n_j)\right)$$

and

$$\mathbf{F}^n_{j+1/2} = \frac{1}{\Delta t}\int_{t_n}^{t_{n+1}} \mathbf{f}\left(\mathbf{u}^*(\mathbf{U}^n_{j}, \mathbf{U}^n_{j+1})\right)\,\mathrm{d}t = \mathbf{f}\left(\mathbf{u}^*(\mathbf{U}^n_{j}, \mathbf{U}^n_{j+1})\right).$$

This part follows the usual description of the Godunov method and the function $\mathbf{f}(\mathbf{u}^*(\mathbf{u}_L, \mathbf{u}_R))$ may be evaluated based on the construction of the solution of the Riemann problem.

It remains to evaluate the integral of the nozzling terms in (28). In view of the components of $\mathbf{h}(\mathbf{u})$, we must examine the three integrals

$$I_1 = \frac{1}{\Delta x}\int_{t_n}^{t_{n+1}}\int_{x_{j-1/2}}^{x_{j+1/2}} \bar{v}\bar{\alpha}_x\,\mathrm{d}x\,\mathrm{d}t, \quad I_2 = \frac{1}{\Delta x}\int_{t_n}^{t_{n+1}}\int_{x_{j-1/2}}^{x_{j+1/2}} p\bar{\alpha}_x\,\mathrm{d}x\,\mathrm{d}t,$$

and

$$I_3 = \frac{1}{\Delta x}\int_{t_n}^{t_{n+1}}\int_{x_{j-1/2}}^{x_{j+1/2}} p\bar{v}\bar{\alpha}_x\,\mathrm{d}x\,\mathrm{d}t.$$

Each integration is carried out over the grid cell Ω_j^n as shown in Fig. 9. For example, suppose that the solid contact from the Riemann problem centered at $x_{j-1/2}$ (labeled $\bar{C}_{j-1/2}$ in the figure) enters the cell from the left with constant velocity $\bar{v}^n_{c,j-1/2} > 0$. There are other waves associated with this Riemann problem (and the Riemann problem centered at $x_{j+1/2}$), but they are not essential to the evaluation of the integrals since $\bar{\alpha}$ is constant across them. We suppose further that the solid contact from the Riemann problem centered at $x_{j+1/2}$ has a positive velocity so it is outside the grid cell of interest. In Ω_j^n, $\bar{\alpha}(x,t)$ equals $\bar{\alpha}^n_{j-1}$ to the left of a

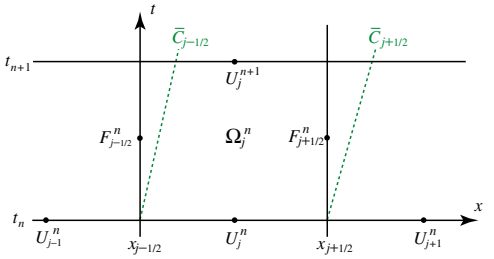

Fig. 9. Grid cell Ω_j^n with solid contact $\bar{C}_{j-1/2}$ from the Riemann problem at $x_{j-1/2}$.

thin layer about $\overline{C}_{j-1/2}$ and it equals $\bar{\alpha}_j^n$ to the right of the layer. Since $\bar{v} = \text{constant} = \bar{v}_{c,j-1/2}^n$ across the layer, the scalar integrals reduce to

$$I_1 = \frac{\Delta t}{\Delta x}\bar{v}_{c,j-1/2}^n(\bar{\alpha}_j^n - \bar{\alpha}_{j-1}^n), \quad I_2 = \frac{\Delta t}{\Delta x}\int_{\xi_{j-1/2}^-}^{\xi_{j-1/2}^+} p\bar{\alpha}_\xi \, \mathrm{d}\xi,$$

and

$$I_3 = \bar{v}_{c,j-1/2}^n I_2,$$

where $\xi = \xi_{j-1/2}$ denotes the center of the thin layer about $\overline{C}_{j-1/2}$. The final integral may be evaluated using (13). We find

$$\int_{\xi_{j-1/2}^-}^{\xi_{j-1/2}^+} p\bar{\alpha}_\xi \, \mathrm{d}\xi = \int_{\xi_{j-1/2}^-}^{\xi_{j-1/2}^+} (\bar{p}\bar{\alpha})_\xi \, \mathrm{d}\xi = \bar{p}_{2,j-1/2}^n\bar{\alpha}_j^n - \bar{p}_{1,j-1/2}^n\bar{\alpha}_{j-1}^n,$$

where $\bar{p}_{1,j-1/2}^n$ and $\bar{p}_{2,j-1/2}^n$ are the solid pressures on either side of $\overline{C}_{j-1/2}$ as determined by the solution of the Riemann problem centered at $x_{j-1/2}$ (e.g., the pressures $\bar{p}_1$ and $\bar{p}_2$ in Fig. 2(a)). The integral of the nozzling terms becomes path independent locally about each solid contact layer within the piecewise constant construction of the Godunov method (and our thin-layer assumption).

The integral of the nozzling terms in (28) with components given by I_1, I_2 and I_3 provides non-conservative contributions to the standard Godunov flux $\mathbf{f}(\mathbf{u}^*(\mathbf{U}_{j-1}^n, \mathbf{U}_j^n))$ depending on the sign of $\bar{v}_{c,j-1/2}^n$. We find it convenient to define

$$\mathbf{H}(\mathbf{U}_{j-1}^n, \mathbf{U}_j^n) = \begin{bmatrix} -\bar{v}_{c,j-1/2}^n(\bar{\alpha}_j^n - \bar{\alpha}_{j-1}^n) \\ 0 \\ +(\bar{p}_{2,j-1/2}^n\bar{\alpha}_j^n - \bar{p}_{1,j-1/2}^n\bar{\alpha}_{j-1}^n) \\ +\bar{v}_{c,j-1/2}^n(\bar{p}_{2,j-1/2}^n\bar{\alpha}_j^n - \bar{p}_{1,j-1/2}^n\bar{\alpha}_{j-1}^n) \\ 0 \\ -(\bar{p}_{2,j-1/2}^n\bar{\alpha}_j^n - \bar{p}_{1,j-1/2}^n\bar{\alpha}_{j-1}^n) \\ -\bar{v}_{c,j-1/2}^n(\bar{p}_{2,j-1/2}^n\bar{\alpha}_j^n - \bar{p}_{1,j-1/2}^n\bar{\alpha}_{j-1}^n) \end{bmatrix}, \tag{30}$$

and then set

$$\mathbf{F}_{\mathrm{L}}(\mathbf{U}_{j-1}^n, \mathbf{U}_j^n) = \begin{cases} \mathbf{f}(\mathbf{u}^*(\mathbf{U}_{j-1}^n, \mathbf{U}_j^n)) - \mathbf{H}(\mathbf{U}_{j-1}^n, \mathbf{U}_j^n) & \text{if } \bar{v}_{c,j-1/2}^n < 0, \\ \mathbf{f}(\mathbf{u}^*(\mathbf{U}_{j-1}^n, \mathbf{U}_j^n)) & \text{if } \bar{v}_{c,j-1/2}^n > 0, \end{cases} \tag{31}$$

and

$$\mathbf{F}_{\mathrm{R}}(\mathbf{U}_{j-1}^n, \mathbf{U}_j^n) = \begin{cases} \mathbf{f}(\mathbf{u}^*(\mathbf{U}_{j-1}^n, \mathbf{U}_j^n)) & \text{if } \bar{v}_{c,j-1/2}^n < 0, \\ \mathbf{f}(\mathbf{u}^*(\mathbf{U}_{j-1}^n, \mathbf{U}_j^n)) + \mathbf{H}(\mathbf{U}_{j-1}^n, \mathbf{U}_j^n) & \text{if } \bar{v}_{c,j-1/2}^n > 0. \end{cases} \tag{32}$$

Here, $\mathbf{F}_{\mathrm{L}}(\mathbf{U}_{j-1}^n, \mathbf{U}_j^n)$ is the combined numerical flux applied to cell Ω_{j-1}^n to the left of $x_{j-1/2}$ while $\mathbf{F}_{\mathrm{R}}(\mathbf{U}_{j-1}^n, \mathbf{U}_j^n)$ is the combined numerical flux applied to cell Ω_j^n to the right. One of these two fluxes picks up the contribution from the non-conservative terms depending on the direction of $\overline{C}_{j-1/2}$ as determined by the sign of $\bar{v}_{c,j-1/2}^n$.

We may now write our finite-volume Godunov scheme for the model equations. It takes the compact form

$$\mathbf{U}_j^{n+1} = \mathbf{U}_j^n - \frac{\Delta t}{\Delta x}\Big(\mathbf{F}_{\mathrm{L}}(\mathbf{U}_j^n, \mathbf{U}_{j+1}^n) - \mathbf{F}_{\mathrm{R}}(\mathbf{U}_{j-1}^n, \mathbf{U}_j^n)\Big), \tag{33}$$

where the numerical flux functions $\mathbf{F}_L$ and $\mathbf{F}_R$ are given by (31) and (32), respectively. The evaluation of the numerical flux functions relies on solutions of the Riemann problem. A procedure to obtain the full solution involves a two-stage iterative procedure as discussed previously. While this full solution is required for accuracy for certain left and right states, an approximate solution requiring much less computational cost is suitable in most cases. In Section 5, we describe an adaptive Riemann solver which handles both cases, and is used to evaluate $\mathbf{F}_L$ and $\mathbf{F}_R$ accurately and efficiently.

Before leaving this section, we note the behavior of (33) corresponding to two special solutions of (1). The first solution is the decoupled phase case when $\bar{\alpha} = \text{constant}$. Here, if $\bar{\alpha}_j^n$ is constant for all j, then the first components of both $\mathbf{F}_L$ and $\mathbf{F}_R$ vanish so that $\bar{\alpha}_j^{n+1} = \bar{\alpha}_j^n$. Further, $\bar{p}_1 = \bar{p}_2 = \bar{p}_*$ when $\bar{\alpha}_L = \bar{\alpha}_R$ (see Section 3.2) so that $\mathbf{H} = 0$ and the fluxes $\mathbf{F}_L$ and $\mathbf{F}_R$ reduce to the standard Godunov fluxes for the discrete solid phase and gas phase variables separately. A second special solution occurs when $p = \bar{p} = \text{constant} = P$ and $v = \bar{v} = \text{constant} = V$, the so-called free-streaming solution. In this solution, $\bar{\alpha}$, $\bar{\alpha}\bar{\rho}$ and $\alpha\rho$ each evolve according to linear advection equations with characteristic velocity equal to V. For this case, if we consider $p_j^n = \bar{p}_j^n = P$ and $v_j^n = \bar{v}_j^n = V$ for all j (at some n), then all Riemann problems would be solved with $p = \bar{p} = P$ and $v = \bar{v} = V$ for all states, and $(\bar{\alpha}^*, \bar{\rho}^*, \rho^*)$ equal to $(\bar{\alpha}_L, \bar{\rho}_L, \rho_L)$ if $V > 0$ and equal to $(\bar{\alpha}_R, \bar{\rho}_R, \rho_R)$ if $V < 0$. Assuming the case $V > 0$, for example, it is straightforward to show that (33) reduces to $p_j^{n+1} = \bar{p}_j^{n+1} = P$ and $v_j^{n+1} = \bar{v}_j^{n+1} = V$, and

$$\begin{aligned}
\bar{\alpha}_j^{n+1} &= \bar{\alpha}_j^n - \sigma\left(\bar{\alpha}_j^n - \bar{\alpha}_{j-1}^n\right),\\
\bar{\alpha}_j^{n+1}\bar{\rho}_j^{n+1} &= \bar{\alpha}_j^n\bar{\rho}_j^n - \sigma\left(\bar{\alpha}_j^n\bar{\rho}_j^n - \bar{\alpha}_{j-1}^n\bar{\rho}_{j-1}^n\right),\\
\alpha_j^{n+1}\rho_j^{n+1} &= \alpha_j^n\rho_j^n - \sigma\left(\alpha_j^n\rho_j^n - \alpha_{j-1}^n\rho_{j-1}^n\right),
\end{aligned}$$

where $\sigma = V\Delta t/\Delta x$. Thus, uniform pressure and velocity is maintained exactly in the numerical approximation of the free-streaming solution and $\bar{\alpha}_j^n$, $\bar{\alpha}_j^n\bar{\rho}_j^n$ and $\alpha_j^n\rho_j^n$ evolve according to first-order upwind methods as expected.

5. An adaptive Riemann solver

The solution of the Riemann problem requires an iterative procedure (in general) and we have described a two-stage process based on Newton's method in Section 3.2. This solution provides the basis for our Godunov method in (33), but it is usually desirable to consider approximate solutions in order to reduce computational cost as mentioned previously. In this section, we discuss suitable approximations for both stages of the iteration and a simple adaptive procedure which chooses whether the approximate solution is sufficient or whether a full iterative solution is desirable. We begin in Section 5.1 with a brief description of an approximation of the decoupled "star" states followed in Section 5.2 with a discussion of a linear approximation of the jump conditions at the solid contact and a simple criterion which we use to determine when the approximate solution is suitable.

5.1. Approximate star states

The first stage of the iterative process involves the solution of Riemann problems for the Euler equations for each phase separately. Since the solution of these decoupled problems is needed only as an initial guess for the Newton iteration in the second stage, an approximate solution is sufficient. There are many approximate Riemann solvers for the Euler equations that may be used for this task, but it is convenient to use the approximate-state Riemann solver suggested by Toro since it involves several formulas and constants used

in the approximation of the second stage. We outline briefly the relevant formulas for completeness here, a full description appears elsewhere (cf. [24, Chapter 9]).

Let us consider the Riemann problem for the Euler equations with left and right states given by (ρ_L, v_L, p_L) and (ρ_R, v_R, p_R), respectively, either for the gas or solid variables. If the states are close to one another, then a linearization is appropriate which results in the formula

$$p_{*,\mathrm{lin}} = \frac{1}{2}(p_L + p_R) + \frac{1}{8}(\rho_L + \rho_R)(a_L + a_R)(v_L - v_R). \tag{34}$$

In order to determine whether or not the linearization in (34) is suitable, Toro suggests the checks

$$\frac{p_{\max}}{p_{\min}} < Q_{\mathrm{user}} \quad \text{and} \quad p_{\min} < \tilde{p}_{*,\mathrm{lin}} < p_{\max}, \tag{35}$$

where $p_{\min} = \min\{p_L, p_R\}$, $p_{\max} = \max\{p_L, p_R\}$ and Q_{user} is a user-defined parameter whose value is taken to be 2. If both conditions in (35) are satisfied, then $p_{*,\mathrm{lin}}$ is considered to be an accurate approximation for p_*. If either of the conditions is violated, then alternate approximations are used. For example, Toro suggests the value

$$p_{*,\mathrm{tr}} = \left[\frac{a_L + a_R - \frac{1}{2}(\gamma - 1)(v_R - v_L)}{a_L p_L^{-(\gamma-1)/2\gamma} + a_R p_R^{-(\gamma-1)/2\gamma}}\right]^{2\gamma/(\gamma-1)} \tag{36}$$

given by the two-rarefaction solution of the Riemann problem if $p_{*,\mathrm{lin}} < p_{\min}$, and the value

$$p_{*,\mathrm{ts}} = \frac{p_L\left(\frac{A_L}{p_{*,\mathrm{lin}} + B_L}\right)^{1/2} + p_R\left(\frac{A_R}{p_{*,\mathrm{lin}} + B_R}\right)^{1/2} - v_R + v_L}{\left(\frac{A_L}{p_{*,\mathrm{lin}} + B_L}\right)^{1/2} + \left(\frac{A_R}{p_{*,\mathrm{lin}} + B_R}\right)^{1/2}} \tag{37}$$

given by an approximation of the two-shock solution if $p_{*,\mathrm{lin}} \geqslant p_{\min}$. In the two-shock formula, A_s and B_s, $s = \mathrm{L}$ or R, are given in (8) and $p_{*,\mathrm{lin}}$ is given in (34).

An approximate value for p_* is thus given by (34), (36) or (37) depending on the various conditions mentioned above. Using this value, we may compute the starred velocity using

$$v_* = \frac{1}{2}(v_L + v_R) + \frac{1}{2}(F_R(p_*) - F_L(p_*)). \tag{38}$$

Analogous formulas are used for the solid phase, but with p replaced by $\bar{p} + \bar{p}_0$ for all pressures in (34)–(37) and with bar superscripts added to the remaining variables, which give approximate values for $\bar{p}_*$ and $\bar{v}_*$.

If $|\bar{\alpha}_R - \bar{\alpha}_L|$ is sufficiently small (less than 10^{-3} in our calculations), then we may stop here and use the approximate values for $(p_*, \bar{p}_*)$ and $(v_*, \bar{v}_*)$ to obtain $\mathbf{f}(\mathbf{u}^*(\mathbf{u}_L, u_R))$ for the (decoupled) Godunov fluxes in (33). If the difference is not approximately zero, then we must move on and consider an approximation of the coupled problem as is discussed next.

5.2. Linearized solid contact

The coupling between phases in the Riemann problem occurs at the solid contact which requires the solution of a set of nonlinear algebraic equations given by (22) for the case when both the left and right states contain a mixture of the two phases. If the left and right states come from neighboring grid cells in a numerical solution of a smooth flow, then the jump in the volume fraction between the states would typically be small. Thus, it is reasonable to consider an approximation of the solid contact jump conditions in the limit of small $|\bar{\alpha}_R - \bar{\alpha}_L|$ and then use the resulting approximate values for the intermediate pressures

$(p_1, p_2, \bar{p}_1, \bar{p}_2)$ as a means to obtain $\mathbf{f}(\mathbf{u}^*(\mathbf{u}_L, \mathbf{u}_R))$. This exercise also provides useful information regarding the solvability of the solid contact jump conditions in general.

When $\bar{\alpha}_L = \bar{\alpha}_R$, a solution of (22) is given by

$$p_1 = p_2 = p_*, \quad \bar{p}_1 = \bar{p}_2 = \bar{p}_*,$$

where p_* and $\bar{p}_*$ are the exact star states defined by the pair of equations in (24). For $|\bar{\alpha}_R - \bar{\alpha}_L|$ small, we seek a solution to the jump conditions about an intermediate volume fraction $\bar{\alpha}_m$, say, in the form

$$p_k = p_* + \delta_k, \quad \bar{p}_k = \bar{p}_* + \bar{\delta}_k, \quad k = 1 \text{ and } 2, \tag{39}$$

where δ_k and $\bar{\delta}_k$ are small perturbations to the starred pressures. We may pick $\bar{\alpha}_m$ to be the left or right value of the volume fraction of the solid, or perhaps an average. For our calculations, we take $\bar{\alpha}_m$ to be $\bar{\alpha}_L$, $\bar{\alpha}_R$ or $\frac{1}{2}(\bar{\alpha}_L + \bar{\alpha}_R)$ whichever value is closest to 0.5. Substituting (39) into (22) gives

$$\bar{F}'_L(\bar{p}_*)\bar{\delta}_1 + \bar{F}'_R(\bar{p}_*)\bar{\delta}_2 = 0, \tag{40}$$

$$\alpha_m\left[\left(F'_L(p_*)\delta_1 + F'_R(p_*)\delta_2\right) + \frac{\Delta v_*}{\gamma p_*}(\delta_2 - \delta_1)\right] + \Delta v_*(\alpha_R - \alpha_L) = 0, \tag{41}$$

$$\bar{\alpha}_m\left(\bar{\delta}_2 - \bar{\delta}_1\right) - \Delta p_*(\bar{\alpha}_R - \bar{\alpha}_L) = 0, \tag{42}$$

$$\rho_* \Delta v_*\left(F'_L(p_*)\delta_1 + F'_R(p_*)\delta_2\right) + \delta_2 - \delta_1 = 0, \tag{43}$$

to leading order. Here,

$$\alpha_m = 1 - \bar{\alpha}_m, \quad \Delta v_* = v_* - \bar{v}_*, \quad \Delta p_* = p_* - \bar{p}_*,$$

and

$$\rho_* = \begin{cases} G_L(p_*) & \text{if } v_* > \bar{v}_*, \\ G_R(p_*) & \text{if } v_* < \bar{v}_*. \end{cases} \tag{44}$$

Also,

$$F'_s(p_*) = \begin{cases} \left(1 - \frac{p_* - p_s}{2(B_s + p_*)}\right)\left[\frac{A_s}{p_* + B_s}\right]^{1/2} & \text{if } p_* > p_s \text{ (shock)}, \\ \frac{1}{\rho_s a_s}\left(\frac{p_*}{p_s}\right)^{-(\gamma+1)/2\gamma} & \text{if } p_* < p_s \text{ (rarefaction)}, \end{cases} \tag{45}$$

for $s = L$ or R according to (6), and

$$\bar{F}'_s(\bar{p}_*) = \begin{cases} \left(1 - \frac{\bar{p}_* - \bar{p}_s}{2(\bar{B}_s + \bar{p}_* + \bar{p}_0)}\right)\left[\frac{\bar{A}_s}{\bar{p}_* + \bar{p}_0 + \bar{B}_s}\right]^{1/2} & \text{if } \bar{p}_* > \bar{p}_s \text{ (shock)}, \\ \frac{1}{\bar{\rho}_s \bar{a}_s}\left(\frac{\bar{p}_* + \bar{p}_0}{\bar{p}_s + \bar{p}_0}\right)^{-(\bar{\gamma}+1)/2\bar{\gamma}} & \text{if } \bar{p}_* < \bar{p}_s \text{ (rarefaction)}, \end{cases} \tag{46}$$

according to (9).

We note that the four linear equations separate into a pair of equations for the solid pressure perturbations $(\bar{\delta}_1, \bar{\delta}_2)$ and a pair of equations for the gas pressure perturbations (δ_1, δ_2). The pair, (40) and (42), for the solid pressure perturbations is uniquely solvable if

$$\bar{\alpha}_m \neq 0 \quad \text{and} \quad \bar{F}'_L(\bar{p}_*) + \bar{F}'_R(\bar{p}_*) \neq 0.$$

The former is satisfied if the solid phase does not vanish and the latter is always satisfied since $\bar{F}'_s > 0$, $s = L$ or R. Assuming a non-vanishing solid phase, a unique solution exists and is given by

$$\begin{aligned}\bar{\delta}_1 &= \frac{-\bar{F}'_{\mathrm{R}}(\bar{p}_*)\Delta p_*}{\bar{F}'_{\mathrm{L}}(\bar{p}_*)+\bar{F}'_{\mathrm{R}}(\bar{p}_*)}\left(\frac{\bar{\alpha}_{\mathrm{R}}-\bar{\alpha}_{\mathrm{L}}}{\bar{\alpha}_m}\right),\\ \bar{\delta}_2 &= \frac{\bar{F}'_{\mathrm{L}}(\bar{p}_*)\Delta p_*}{\bar{F}'_{\mathrm{L}}(\bar{p}_*)+\bar{F}'_{\mathrm{R}}(\bar{p}_*)}\left(\frac{\bar{\alpha}_{\mathrm{R}}-\bar{\alpha}_{\mathrm{L}}}{\bar{\alpha}_m}\right).\end{aligned} \tag{47}$$

Eqs. (41) and (43) determine the gas pressure perturbations. This pair of equations is uniquely solvable if

$$\alpha_m \neq 0 \quad \text{and} \quad \left(\gamma p_* - \rho_* \Delta v_*^2\right)\left(F'_{\mathrm{L}}(p_*)+F'_{\mathrm{R}}(p_*)\right) \neq 0.$$

The first is satisfied if the gas phase is present in the flow, and the second is satisfied if

$$M_*^2 = \frac{\Delta v_*^2}{\gamma p_*/\rho_*} \neq 1,$$

which is true if the subsonic condition is met. Assuming these conditions are satisfied, the unique solution is given by

$$\begin{aligned}\delta_1 &= \frac{\left(1+\rho_*\Delta v_* F'_{\mathrm{R}}(p_*)\right)\Delta v_*}{\left(1-M_*^2\right)\left(F'_{\mathrm{L}}(p_*)+F'_{\mathrm{R}}(p_*)\right)}\left(\frac{\alpha_{\mathrm{L}}-\alpha_{\mathrm{R}}}{\alpha_m}\right),\\ \delta_2 &= \frac{\left(1-\rho_*\Delta v_* F'_{\mathrm{L}}(p_*)\right)\Delta v_*}{\left(1-M_*^2\right)\left(F'_{\mathrm{L}}(p_*)+F'_{\mathrm{R}}(p_*)\right)}\left(\frac{\alpha_{\mathrm{L}}-\alpha_{\mathrm{R}}}{\alpha_m}\right).\end{aligned} \tag{48}$$

The perturbations in the pressures given by (47) and (48) reflect a linearized coupling between the phases and correspond to the corrections provided by the first step in the Newton iteration of the nonlinear equations for the solid contact. These formulas are derived based on an exact star state, but are used in practice with the approximate star state given by (34), (36) or (37) for the pressures and by (38) for the velocities. We may now check the size of the residual,

$$\epsilon = \|\mathbf{N}(p_* + \delta_1, p_* + \delta_2, \bar{p}_* + \bar{\delta}_1, \bar{p}_* + \bar{\delta}_2)\|,$$

to determine whether more Newton steps are required. (We assume that the primitive variables of the flow are dimensionless and properly scaled so that we need not scale the components of $\mathbf{N}$ for this check.) If $\epsilon < 10^{-3}$, then we accept the linearized values and use them to determine $\mathbf{u}^*(\mathbf{u}_{\mathrm{L}}, \mathbf{u}_{\mathrm{R}})$. We also use these values to determine the velocity of the solid contact, $\bar{v}_c$, and the solid pressures on either side $(\bar{p}_1, \bar{p}_2)$, which are needed in our numerical treatment of the nozzling terms in (30). If ϵ is too big, then we take more Newton steps to obtain more accurate values for $(p_1, p_2, \bar{p}_1, \bar{p}_2)$, which requires a higher computational cost. In our numerical experiments, we monitor the number of Newton steps required and find that the linear approximation is sufficient for the majority of Riemann solutions (see Section 7).

Finally, we note that in extreme cases, either when $|\bar{\alpha}_{\mathrm{R}} - \bar{\alpha}_{\mathrm{L}}|$ is close to 1 or when one of the phases nearly vanishes, the Newton iteration may not converge for the initial guess given by the decoupled star states. For such cases, we employ a simple continuation procedure in either the left or right value for $\bar{\alpha}$. For example, suppose $\bar{\alpha}_{\mathrm{L}}$ is closest to 0.5. We fix this value and adjust $\bar{\alpha}_{\mathrm{R}}$ closer to $\bar{\alpha}_{\mathrm{L}}$, while holding the other primitive values in the left and right states fixed, until Newton's method converges. Once convergence occurs, we then slowly move $\bar{\alpha}_{\mathrm{R}}$ back to its original value during the Newton iteration. While this situation rarely occurs (and if so requires only a tiny fraction of the overall computational cost of the method), we find it helpful for a robust implementation of the method.

6. A high-resolution method

The Godunov method described in Section 4 is first order accurate, and may be extended to second order using slope-limited corrections of the left and right states in the Riemann problem. This approach to generate a high-resolution method is well established in the literature for the Euler equations, see [8,9] for example, and has been used in other numerical schemes for compressible multi-phase flow, see [18,19] for example. The description of the second-order extension here follows similar lines except for our treatment of the non-conservative terms which is new. Essentially, the extension for the non-conservative terms involves two parts, one coming from a contribution to the integral of $\mathbf{h}(\mathbf{u})\bar{\alpha}_x$ about the solid contact and the other coming from the integral away from the jump at the solid contact. The latter contribution arises due to the slope correction for $\bar{\alpha}$ as we describe below.

It is convenient to obtain the corrections in terms of the primitive variables $\mathbf{w} = (\bar{\alpha}, \bar{\rho}, \bar{v}, \bar{p}, \rho, v, p)^{\mathrm{T}}$. This may be done using the quasi-linear form of the model which takes the form

$$\mathbf{w}_t + A(\mathbf{w})\mathbf{w}_x = 0,$$

where

$$A(\mathbf{w}) = \begin{bmatrix} \bar{v} & 0 & 0 & 0 & 0 & 0 & 0 \\ 0 & \bar{v} & \bar{\rho} & 0 & 0 & 0 & 0 \\ -\frac{\Delta p}{\bar{\alpha}\bar{\rho}} & 0 & \bar{v} & \frac{1}{\bar{\rho}} & 0 & 0 & 0 \\ 0 & 0 & \bar{\rho}\bar{a}^2 & \bar{v} & 0 & 0 & 0 \\ -\frac{\rho\Delta v}{\alpha} & 0 & 0 & 0 & v & \rho & 0 \\ 0 & 0 & 0 & 0 & 0 & v & \frac{1}{\rho} \\ -\frac{\rho a^2\Delta v}{\alpha} & 0 & 0 & 0 & 0 & \rho a^2 & v \end{bmatrix}, \qquad \begin{aligned} \Delta p &= p - \bar{p}, \\ \Delta v &= v - \bar{v}. \end{aligned}$$

Let us consider the grid cell Ω_j^n defined earlier in Section 4 and let $\mathbf{w}_j^n$ denote the primitive variables corresponding to the cell average $\mathbf{U}_j^n$. First order approximations are needed at cell boundaries. For example, a first order approximation for $\mathbf{w}$ at $(x_{j+1/2}, t_{n+1/2})$ is given by

$$\mathbf{w}_{j,+}^n = \mathbf{w}_j^n + \frac{\Delta x}{2}(\mathbf{w}_x)_j^n + \frac{\Delta t}{2}(\mathbf{w}_t)_j^n = \mathbf{w}_j^n + \frac{1}{2}\left(I - \frac{\Delta t}{\Delta x}A_j^n\right)\Delta\mathbf{w}_j^n, \tag{49}$$

where $A_j^n = A(\mathbf{w}_j^n)$ and $\Delta\mathbf{w}_j^n$ is a discrete approximation of $(\mathbf{w}_x)_j^n\Delta x$. The slope correction in (49) is limited in order to suppress numerical oscillations, and this is done in characteristic variables. Let

$$\Lambda(\mathbf{w}) = \mathrm{diag}(\bar{v}, \bar{v} - \bar{a}, \bar{v}, \bar{v} + \bar{a}, v - a, v, v + a)$$

and

$$R(\mathbf{w}) = \begin{bmatrix} 1 & 0 & 0 & 0 & 0 & 0 & 0 \\ 0 & \bar{\rho} & 1 & \bar{\rho} & 0 & 0 & 0 \\ 0 & -\bar{a} & 0 & \bar{a} & 0 & 0 & 0 \\ \frac{\Delta p}{\bar{\alpha}} & \bar{\rho}\bar{a}^2 & 0 & \bar{\rho}\bar{a}^2 & 0 & 0 & 0 \\ -\frac{\rho\Delta v^2}{\alpha(a^2-\Delta v^2)} & 0 & 0 & 0 & \rho & 1 & \rho \\ \frac{a^2\Delta v}{\alpha(a^2-\Delta v^2)} & 0 & 0 & 0 & -a & 0 & a \\ -\frac{\rho a^2\Delta v^2}{\alpha(a^2-\Delta v^2)} & 0 & 0 & 0 & \rho a^2 & 0 & \rho a^2 \end{bmatrix},$$

so that Λ and R solve $AR = R\Lambda$ and the characteristic variables are $\mathbf{z} = R^{-1}\mathbf{w}$. A slope-limited correction at $(x_{j+1/2}, t_{n+1/2})$ is

$$\mathbf{w}^n_{j,+} = \mathbf{w}^n_j + \frac{1}{2}R^n_j\left(I - \frac{\Delta t}{\Delta x}\max\{\Lambda^n_j, 0\}\right)\Delta\mathbf{z}^n_j, \tag{50}$$

where

$$\Delta\mathbf{z}^n_j = \text{minmod}\left(R^{-1}(\mathbf{w}^n_{j+1} - \mathbf{w}^n_j), R^{-1}(\mathbf{w}^n_j - \mathbf{w}^n_{j-1})\right). \tag{51}$$

Here, the maximum and minimum-modulus functions are performed componentwise. Similar steps give

$$\mathbf{w}^n_{j,-} = \mathbf{w}^n_j - \frac{1}{2}R^n_j\left(I + \frac{\Delta t}{\Delta x}\min\{\Lambda^n_j, 0\}\right)\Delta\mathbf{z}^n_j, \tag{52}$$

which is a slope-limited correction at $(x_{j-1/2}, t_{n+1/2})$. Finally, let $\mathbf{U}^n_{j,\pm}$ denote the conservative variables corresponding to $\mathbf{w}^n_{j,\pm}$.

The slope-limited corrections $\mathbf{U}^n_{j,\pm}$ may now be used to extend (33) to second order. These values provide corrections at cell boundaries which may then be used as left and right states for the Riemann problems. They also provide a slope correction to the integral of the non-conservative terms. For example, consider the Riemann problem about the boundary $x_{j-1/2}$ with left and right states given by $\mathbf{U}^n_{j-1,+}$ and $\mathbf{U}^n_{j,-}$, respectively. The adaptive Riemann solver provides the necessary information to evaluate the numerical fluxes $\mathbf{F}_L(\mathbf{U}^n_{j-1,+}, \mathbf{U}^n_{j,-})$ and $\mathbf{F}_R(\mathbf{U}^n_{j-1,+}, \mathbf{U}^n_{j,-})$ defined by (31) and (32), respectively. These fluxes contain the second-order Godunov flux at the boundary of the cell, $\mathbf{f}(\mathbf{u}^*(\mathbf{U}^n_{j-1,+}, \mathbf{U}^n_{j,-}))$, and the second-order contribution to the integral of the non-conservative terms about the solid contact, $\mathbf{H}(\mathbf{U}^n_{j-1,+}, \mathbf{U}^n_{j,-})$.

It remains to determine the second-order contribution to the integral away from the solid contact. This contribution arises in the second-order extension since $\bar{\alpha}$ involves a slope correction, and thus away from the solid contact $\bar{\alpha}_x \neq 0$ in general. In order to specify this contribution, let us consider the solution of the Riemann problem about the cell boundary $x_{j-1/2}$ and define the pairs $(\bar{v}_{\ell,j-1/2}, p_{\ell,j-1/2})$ and $(\bar{v}_{r,j-1/2}, p_{r,j-1/2})$ as follows:

$$\left.\begin{aligned}(\bar{v}_{\ell,j-1/2}, p_{\ell,j-1/2}) &= (\bar{v}^n_{c,j-1/2}, p^n_{1,j-1/2})\\ (\bar{v}_{r,j-1/2}, p_{r,j-1/2}) &= (\bar{v}^*_{j-1/2}, p^*_{j-1/2})\end{aligned}\right\} \quad \text{if } \bar{v}^n_{c,j-1/2} < 0,$$

and

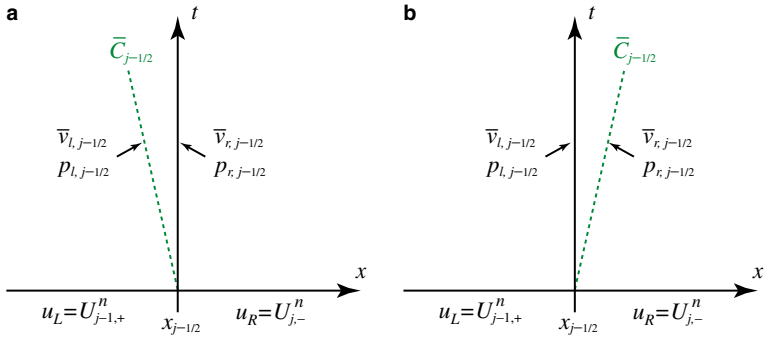

Fig. 10. Values for $(\bar{v}_{\ell,j-1/2}, p_{\ell,j-1/2})$ and $(\bar{v}_{r,j-1/2}, p_{r,j-1/2})$ about $x_{j-1/2}$ for (a) $\bar{v}^n_{c,j-1/2} < 0$ and (b) $\bar{v}^n_{c,j-1/2} > 0$.

$$\left.\begin{aligned}(\bar{v}_{\ell,j-1/2}, p_{\ell,j-1/2}) &= (\bar{v}^*_{j-1/2}, p^*_{j-1/2}) \\ (\bar{v}_{r,j-1/2}, p_{r,j-1/2}) &= (\bar{v}^n_{c,j-1/2}, p^n_{2,j-1/2})\end{aligned}\right\} \quad \text{if } \bar{v}^n_{c,j-1/2} > 0$$

(see Fig. 10). These velocities and pressures may now be used to approximate the integral of the non-conservative terms away from the jump at the solid contact. For the grid cell Ω^n_j, the contribution to the integral is given by

$$\tilde{\mathbf{H}}^n_j = \begin{bmatrix} -\frac{1}{2}(\bar{v}_{r,j-1/2} + \bar{v}_{\ell,j+1/2})\Delta\bar{\alpha}^n_j \\ 0 \\ +\frac{1}{2}(p_{r,j-1/2} + p_{\ell,j+1/2})\Delta\bar{\alpha}^n_j \\ +\frac{1}{2}(p_{r,j-1/2}\bar{v}_{r,j-1/2} + p_{\ell,j+1/2}\bar{v}_{\ell,j+1/2})\Delta\bar{\alpha}^n_j \\ 0 \\ -\frac{1}{2}(p_{r,j-1/2} + p_{\ell,j+1/2})\Delta\bar{\alpha}^n_j \\ -\frac{1}{2}(p_{r,j-1/2}\bar{v}_{r,j-1/2} + p_{\ell,j+1/2}\bar{v}_{\ell,j+1/2})\Delta\bar{\alpha}^n_j \end{bmatrix}, \tag{53}$$

where $\Delta\bar{\alpha}^n_j = \bar{\alpha}^n_{j,+} - \bar{\alpha}^n_{j,-}$. This contribution applies only in smooth regions of the flow (due to the slope limiting) so that the averages used in (53) are suitable.

We now have all of the ingredients for our second-order extension of (33). It has the form

$$\mathbf{U}^{n+1}_j = \mathbf{U}^n_j - \frac{\Delta t}{\Delta x}\left(\mathbf{F}_{\mathrm{L}}(\mathbf{U}^n_{j,+}, \mathbf{U}^n_{j+1,-}) - \mathbf{F}_{\mathrm{R}}(\mathbf{U}^n_{j-1,+}, \mathbf{U}^n_{j,-})\right) + \frac{\Delta t}{\Delta x}\tilde{\mathbf{H}}^n_j, \tag{54}$$

where $\mathbf{F}_{\mathrm{L}}$ and $\mathbf{F}_{\mathrm{R}}$ are defined by (31) and (32), respectively, and $\tilde{\mathbf{H}}^n_j$ is given in (53). As with the first-order method, we note that (54) reduces to a standard slope-limited extension of Godunov's method for the Euler equations for each phase separately when $\bar{\alpha}^n_j$ is constant. Also, it can be shown that the pressure and velocity remain constant in the free-streaming case, and that $\bar{\alpha}^n_j$, $\bar{\alpha}^n_j\bar{\rho}^n_j$ and $\alpha^n_j\rho^n_j$ evolve according to second-order finite difference approximations of their respective linear advection equations (except near local extrema where the approximations become first order due to the slope limiter).

7. Numerical results

In this section, we consider a variety of problems for the governing equations (1) in order to illustrate the behavior and accuracy of our first order Godunov method (33) and its second-order extension (54). We begin by illustrating numerical solutions of the Riemann problems described in Section 3. These problems involve the case where both the left and right states consist of a mixture of the phases and cases where the solid or gas phase vanishes in the left or right states. For the mixture case with left and right states given in Table 1, we perform a careful check of the behavior of the numerical solution through the thin solid contact layer. Next, we compute numerical solutions of the model equations for smooth initial conditions and then use these solutions to perform a grid refinement study. This is done as a means to verify the order of accuracy of the methods. Finally, we compute solutions using two alternate numerical methods suggested by the work in [18,19]. We then compare solutions obtained using these two alternate methods with that given by (33). It is found that the present method gives more accurate results for the test problem used, which we attribute to a more accurate numerical treatment of the non-conservative terms about the solid contact.

Fig. 11 shows numerical solutions and the exact solution at $t = 0.2$ for the Riemann problem with left and right states given in Table 1. The short-dashed blue curve in each plot is obtained using the first-order method while the long-dashed red curve is given by its second-order extension. Both of these numerical solutions are computed using $N = 200$ grid cells and a Δt determined by

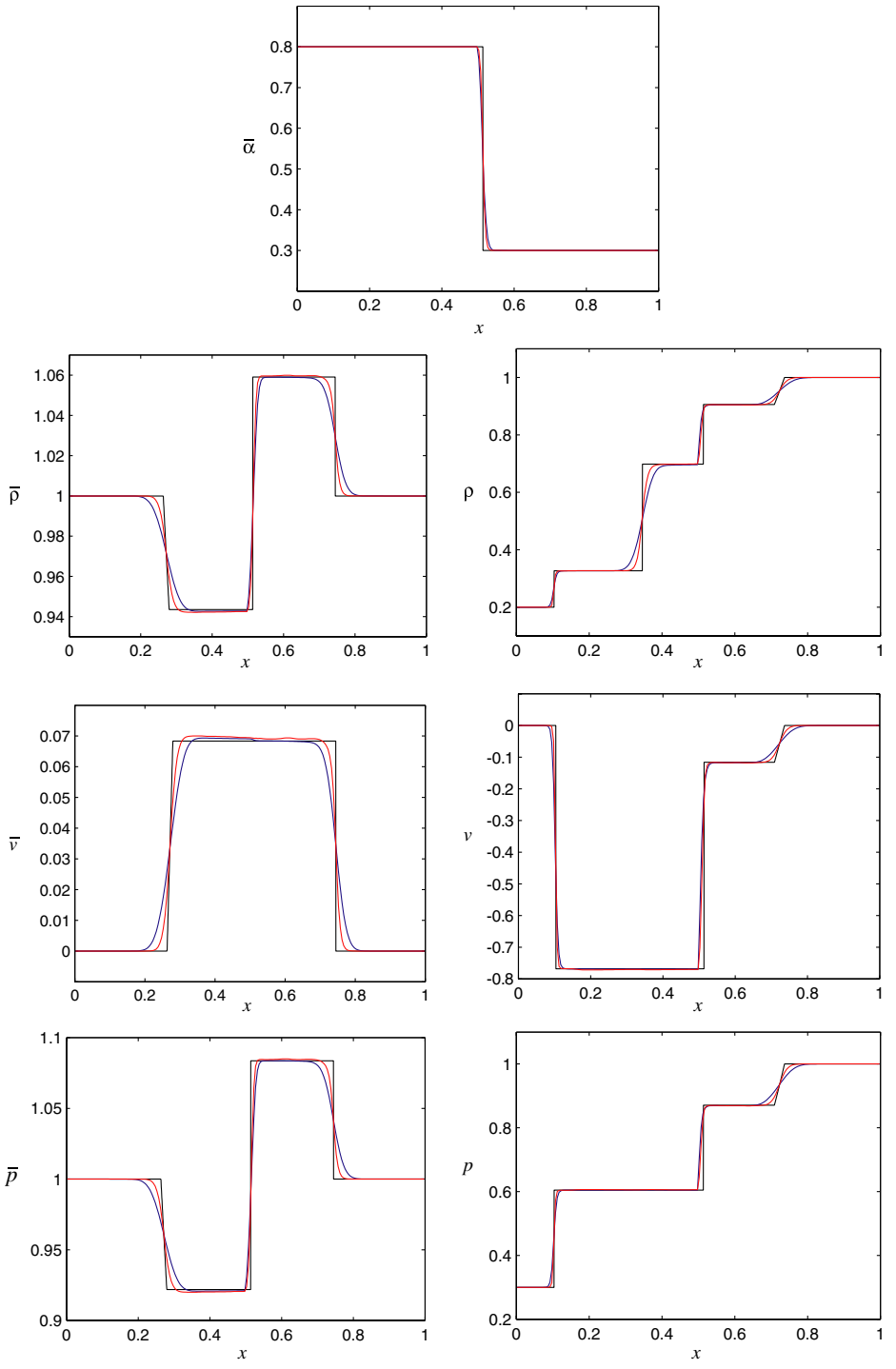

Fig. 11. First-order (short-dashed blue curves) and second-order (long-dashed red curves) numerical solutions at $t = 0.2$ of the Riemann problem with left and right states given in Table 1. The solid black curves indicate the exact solution. (For interpretation of the references to color in this figure legend, the reader is referred to the web version of this article.)

$$\Delta t = 0.8\frac{\Delta x}{\lambda_{\max}}, \quad \lambda_{\max} = \max_{1\leqslant j\leqslant N}\{|\bar{v}_j^n| + \bar{a}_j^n, |v_j^n| + a_j^n\},$$

at each time step. The solid black curve shows the exact solution in each plot. Both numerical solutions are in good agreement with the exact solution, and, as expected, the second-order solution shows less smearing at shocks and contacts, and at the corners of the rarefactions. In particular, we note that both numerical solutions are in good agreement with the exact solution near the solid contact.

The behavior of the numerical solutions near the gas contact, shocks and rarefactions is typical of first-order and (slope-limited) second-order methods for the Euler equations which applies in regions of the flow where $|\bar{\alpha}_j^n - \bar{\alpha}_{j-1}^n|$ is approximately zero. Near the solid contact, on the other hand, where $\bar{\alpha}_j^n$ varies, we may compare the behavior of the numerical solutions with that determined by the jump conditions for the solid contact layer (see Section 3.1). Fig. 12 shows the first-order and second-order solutions at $t = 0.2$ for $\bar{p}$, ρ, v and p versus $\bar{\alpha}$ through the layer. The solid curve is given by layer equations

$$\begin{aligned} &\alpha\rho(v-\bar{v}) = K_1, \quad \alpha\rho(v-\bar{v})^2 + \alpha p + \bar{\alpha}\bar{p} = K_2, \\ &\frac{\gamma p}{(\gamma-1)\rho} + \frac{1}{2}(v-\bar{v})^2 = K_3, \quad \frac{p}{\rho^\gamma} = K_4, \quad \bar{\alpha} + \alpha = 1, \end{aligned} \tag{55}$$

for $\bar{\alpha}$ between 0.3 and 0.8 using the exact state at $\bar{\alpha} = 0.3$ to determine the four constants, K_i, $i = 1,\ldots,4$. The plots show that the numerical solutions agree very well with the solution of the thin layer equations,

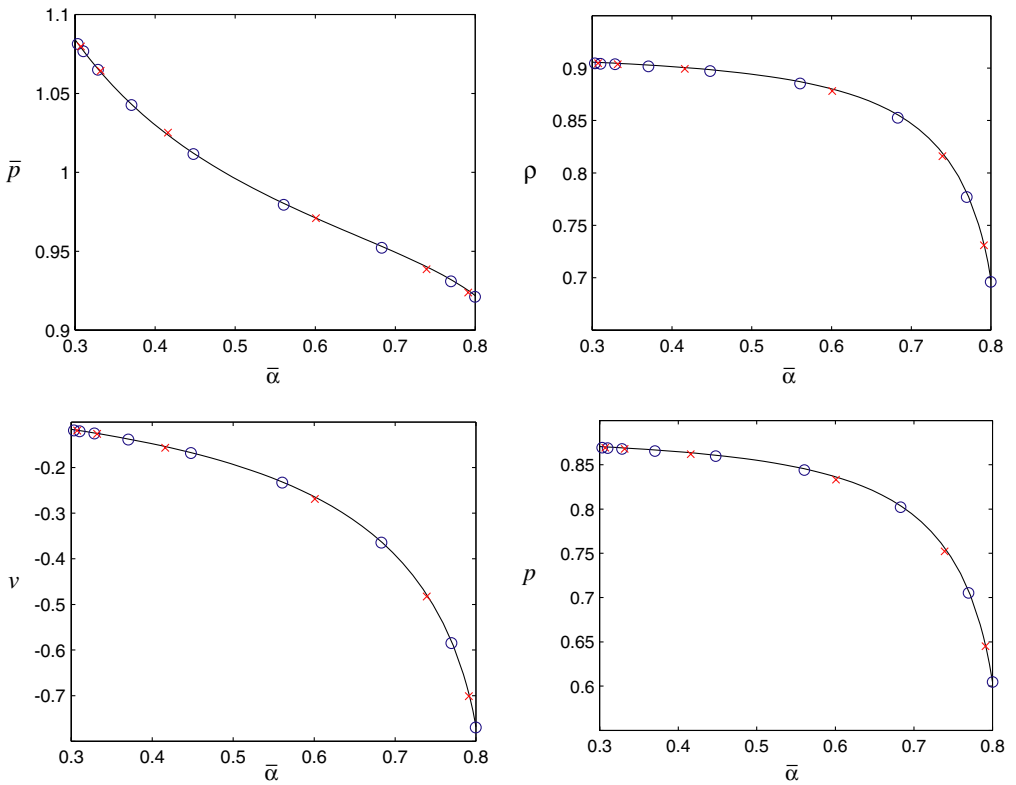

Fig. 12. Behavior of $\bar{p}$, ρ, v and p versus $\bar{\alpha}$ through the solid contact layer for the solution at $t = 0.2$ of the Riemann problem with left and right states given in Table 1. The circles are the first-order solution and the crosses are the second-order solution.

and this is a result of our numerical treatment of the integral of the non-conservative terms over each grid cell, and in particular across the solid contact layer.

The adaptive Riemann solver described in Section 5 is used to perform the Godunov flux calculations for both the first-order and second-order methods. The solver is designed to detect and handle both coupled ($\bar{\alpha}_x \neq 0$) and decoupled ($\bar{\alpha}_x = 0$) flows and take advantage of the computational savings in the flux calculation for decoupled (Euler) flows. In the coupled case, the adaptive solver first considers the linearized equations for the solid contact and checks whether a solution based on this simpler set of equations is sufficient. If the solution is not sufficiently accurate, then additional Newton iterations are performed at an increased computational cost. For example, the second-order solution shown in Figs. 11 and 12 required 24,120 flux calculations. The majority of these flux calculations, approximately 97.6%, were regarded as decoupled. Of the remaining 2.4%, 339 flux calculations were performed based on the linearized equations for the solid contact, while only 246 flux calculations required further Newton iterations (with no continuation in $\bar{\alpha}$). These percentages are representative of numerical solutions in which the coupling between phases is confined to a thin region of x and the jump in $\bar{\alpha}$ is moderate. For other calculations, such as the smooth solution considered later, the coupled flow region is broader, in which case the numerical fluxes may be computed based on the decoupled equations or the linearized coupled equations alone.

As an added check of the numerical approach, we consider a case in which there is a large variation in the values between the left and right states and between the solid and gas phases. Fig. 13 shows the exact solution and numerical solutions for the Riemann problem with left and right states given by

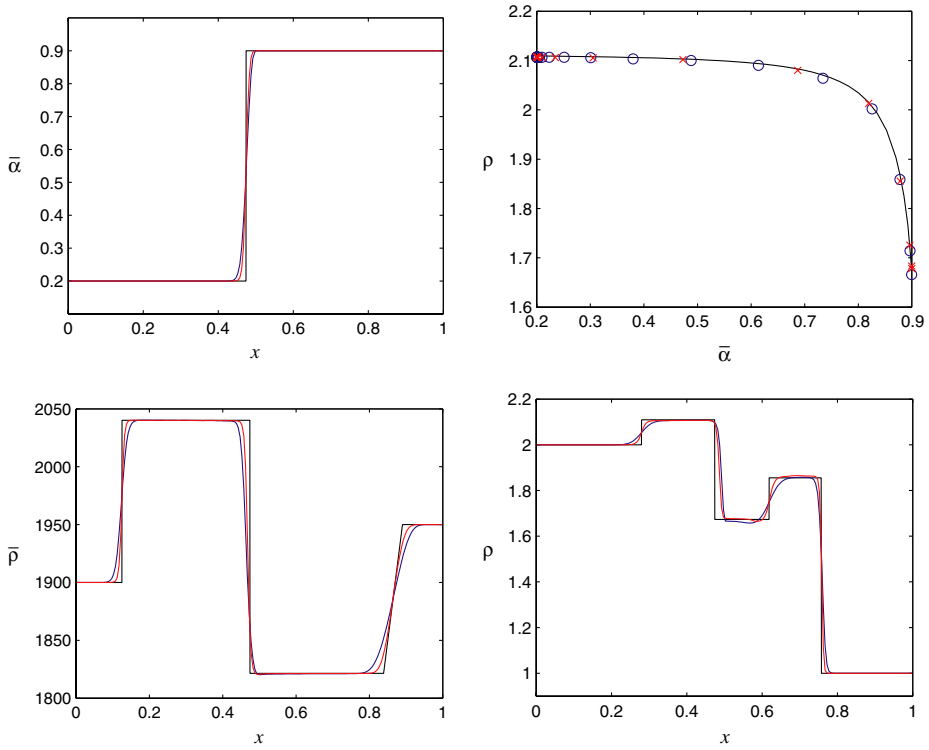

Fig. 13. First-order (short-dashed blue curves) and second-order (long-dashed red curves) numerical solutions at $t = 0.15$ of the Riemann problem with left and right states given in (56) and with $\gamma = 1.35$, $\bar{\gamma} = 3$ and $\bar{p}_0 = 3400$. (For interpretation of the references to color in this figure legend, the reader is referred to the web version of this article.)

$$\begin{aligned}&\bar{\alpha}_L = 0.2, \quad \bar{\rho}_L = 1900, \quad \bar{v}_L = 0, \quad \bar{p}_L = 10, \quad \rho_L = 2, \quad v_L = 0, \quad p_L = 3,\\ &\bar{\alpha}_R = 0.9, \quad \bar{\rho}_R = 1950, \quad \bar{v}_R = 0, \quad \bar{p}_R = 1000, \quad \rho_R = 1, \quad v_R = 0, \quad p_R = 1.\end{aligned} \tag{56}$$

For this case, the equation of state for the gas is specified by $\gamma = 1.35$, while $\bar{\gamma} = 3$ and $\bar{p}_0 = 3400$ are used in the stiffened equation of state for the solid. The values for density and pressure are representative of the ones used in [11–13] and in the recent paper by Powers [26], and the parameters for the equations of state are representative of ones for granular explosives. The plots of $\bar{\alpha}$, $\bar{\rho}$ and ρ versus x show very good agreement between the numerical solutions and the exact solution. The plot of the density of the gas, ρ, versus $\bar{\alpha}$ through the solid contact layer shows very good agreement as well. Overall, the numerical scheme performs very well for this case in view of the large variation in the values of the left and right states including the large jump in the volume fraction of the mixture.

A solution in which the solid or gas phase vanishes may be handled numerically by computing a corresponding approximate solution where the phase nearly vanishes. We may illustrate this by considering the solutions of the two Riemann problems described in Section 3 in which the solid phase vanishes in one of the solutions and the gas phase vanishes in the other. For example, Fig. 14 shows the first-order and second-order numerical solutions at $t = 0.15$ of the Riemann problem with the left state given in Table 2 and a right state given by

$$\bar{\alpha}_R = 10^{-6}, \quad \bar{\rho}_R = 1.7829, \quad \bar{v}_R = 0.2972, \quad \bar{p}_R = 3.5422, \quad \rho_R = 1.8, \quad v_R = 0, \quad p_R = 4. \tag{57}$$

A very small positive value for $\bar{\alpha}_R$ is taken in the right state to maintain a mixture of the phases as required by the numerical method and to approximate the exact solution where $\bar{\alpha}_R = 0$. No values are needed for $\bar{\rho}_R$, $\bar{v}_R$ and $\bar{p}_R$ in the exact problem but some values are needed by the numerical method, and the choice given above is taken from the exact solution for the solid phase in the constant state to the left of the solid contact (Region 1 in Table 2). This choice is not essential but is made here for convenience as it (approximately) eliminates the variation in $\bar{\rho}$, $\bar{v}$ and $\bar{p}$ through the solid contact in the numerical solution and any shock or rarefaction in the C_+ characteristic field to the right of the solid contact. Other choices for $\bar{\rho}_R$, $\bar{v}_R$ and $\bar{p}_R$ could be made, but this would have a negligible effect on the numerical solution for the solid phase variables to the left of the solid contact and on the numerical solution for the gas phase variables on either side of the solid contact. In Fig. 14, the exact position of the solid contact separating the mixture on the left from the gas on the right is marked by a dashed line. Here, we note that the numerical solutions for the solid and gas phase variables agree well with the exact solution on the mixture side of the solid contact, and the gas phase variables agree well to the right of the solid contact. There are small errors in the solid phase variables to the right of the solid contact where the volume fraction is approximately zero. These errors are generated in the first few time steps of the numerical solutions due to the initial jump in the state, but are not considered significant since the volume fraction of the solid is approximately zero there.

An exact solution of the Riemann problem for a case in which the gas phase vanishes in left state is given in Table 3. Numerical solutions for this case may be computed using the left state given by

$$\bar{\alpha}_L = 1 - 10^{-6}, \quad \bar{\rho}_L = 120, \quad \bar{v}_L = 0, \quad \bar{p}_L = 200, \quad \rho_L = 2.7146, \quad v_L = 0.4613, \quad p_L = 4.6166, \tag{58}$$

and the right state given in Table 3. Here, we choose the gas variables in the left state to be those given by the exact solution to the right of the solid contact. As before, this choice is made for convenience but is not essential. Fig. 15 shows the first-order and second-order numerical solutions at $t = 0.15$ for this case, and again we note good agreement between the numerical solutions and the exact solution (apart from small errors in the gas phase variables where $\bar{\alpha}$ is approximately one). In general, we find good agreement for all of our numerical experiments with solutions of Riemann problems.

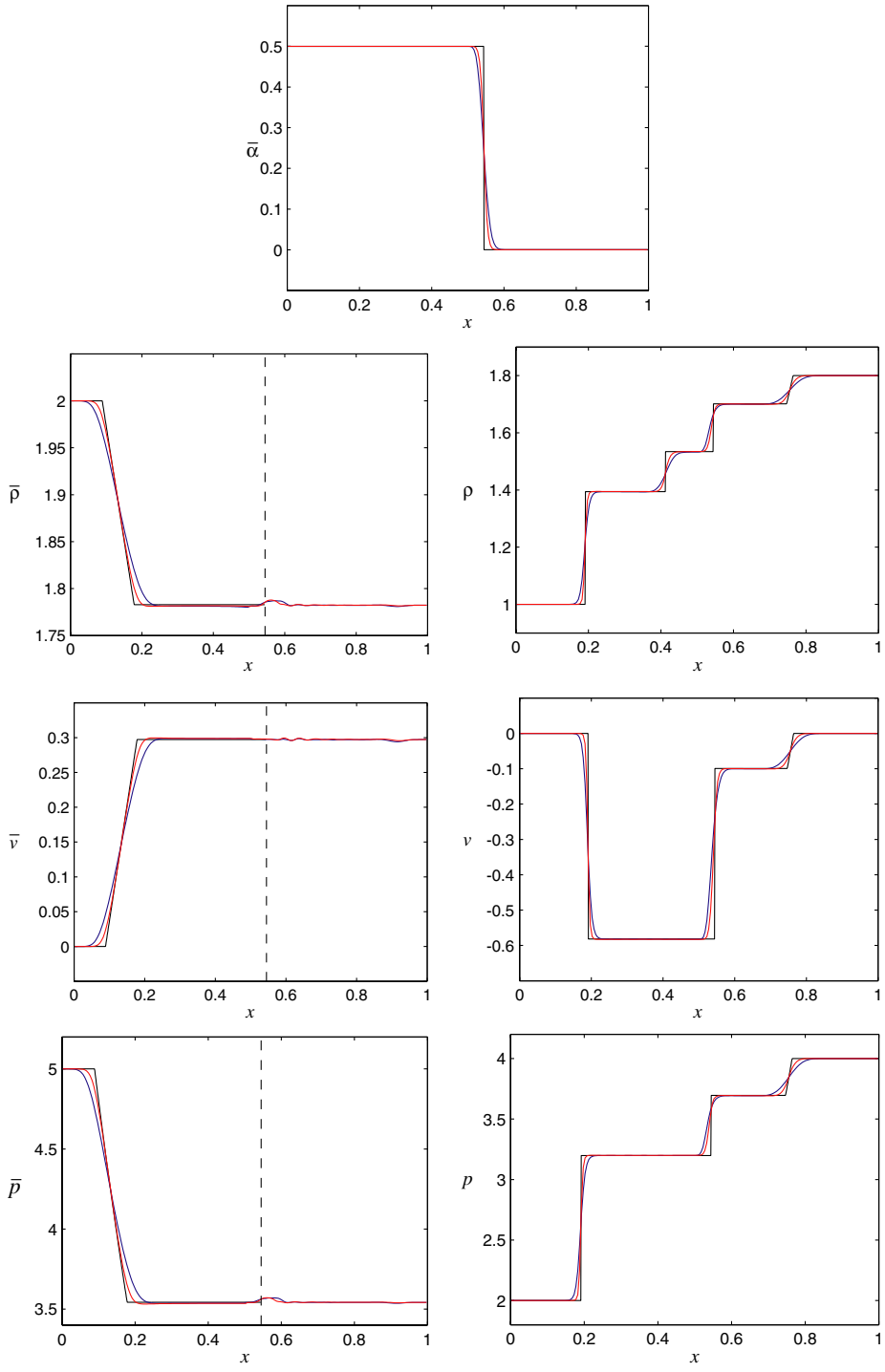

Fig. 14. First-order (short-dashed blue curves) and second-order (long-dashed red curves) numerical solutions at $t = 0.15$ of the Riemann problem with left state given in Table 2 and right state given in (57). Solid black curves show the exact solution for $\bar{\alpha}_R = 0$ and the position of the solid contact is indicated by the dashed vertical line. (For interpretation of the references to color in this figure legend, the reader is referred to the web version of this article.)

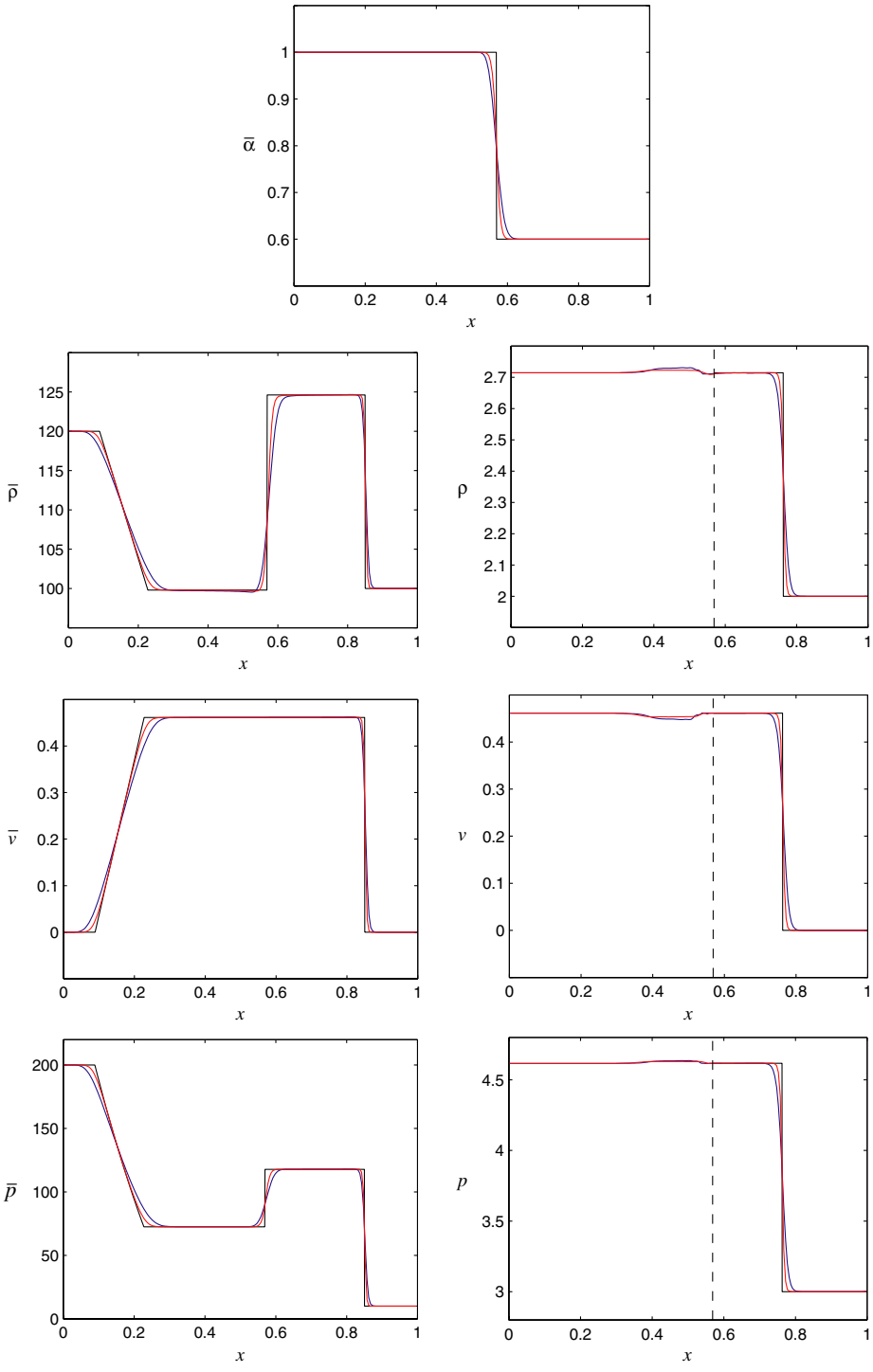

Fig. 15. First-order (short-dashed blue curves) and second-order (long-dashed red curves) numerical solutions at $t = 0.15$ of the Riemann problem with left state given in (58) and right state given in Table 3. Solid black curves show the exact solution for $\bar{\alpha}_L = 1$ and the position of the solid contact is indicated by the dashed vertical line. (For interpretation of the references to color in this figure legend, the reader is referred to the web version of this article.)

Numerical solutions with smooth initial conditions may be computed using the first-order and second-order methods and then used to verify the order of accuracy of the methods. This is done primarily as a further check of our numerical approximation of the non-conservative terms. For example, we take $\gamma = \bar{\gamma} = 1.4$ and $\bar{p}_0 = 0$, and consider the initial conditions

$$\bar{\alpha}(x,0) = \frac{1}{2} + \frac{2}{5}\tanh(20x - 8), \quad \bar{v}(x,0) = \frac{1}{2} + \frac{1}{2}\tanh(20x - 10),$$

and

$$\bar{\rho}(x,0) = \rho(x,0) = 1, \quad \bar{p}(x,0) = p(x,0) = 1, \quad v(x,0) = 0.$$

For these initial conditions, $\bar{\alpha}$ has a smooth transition from 0.1 to 0.9 initially centered at $x = 0.4$, and the solid velocity varies smoothly from 0 on the left to 1 on the right which creates an expansion in the flow initially. The choice of the initial conditions is somewhat arbitrary for the purpose of our grid refinement study, although it is desirable for $\bar{\alpha}(x,0)$ to vary so that the phases are coupled and for the velocity and/or pressure to vary so that the flow is not free-streaming. Unlike the Riemann problems, an exact solution is not available for this problem, but it may be approximated with sufficient accuracy using the second-order numerical method with a very large number of grid cells, e.g., 12,800 grid cells on $x \in [0,1]$ with numerical boundary conditions $\mathbf{U}_0^n = \mathbf{U}_1^n$ and $\mathbf{U}_N^n = \mathbf{U}_{N-1}^n$. Numerical solutions with $N = 100$, 200, 400 and 800 may be computed using our first-order Godunov method (33) and its second-order extension (54) and compared with the highly resolved numerical solution, $\mathbf{u}_j^n$, restricted to the coarser grids. Numerical errors and convergence rates are computed at $t_n = 0.1$ using

$$E_N = \sum_{j=1}^{N} \|\mathbf{U}_j^n - \mathbf{u}_j^n\| \Delta x, \quad r_N = \frac{\ln E_{N/2} - \ln E_N}{\ln 2},$$

respectively, and are presented in Table 4. The convergence rates indicate that our Godunov method, labeled G_1 in the table, is indeed first-order accurate. The convergence rates given by (54), labeled G_2, are slightly smaller than 2 due to the minimum-modulus slope limiter and the presence of local extrema in the solution where the method reduces to first order. If the minmod function in (51) is replaced by an average, then second-order accuracy is achieved as indicated by the convergence rates in the last column of the table. For this problem no shocks or contact discontinuities appear, but in general the slope-limited method would be preferred in order to suppress numerical oscillations when these sharp features occur.

Finally, it is interesting to compare the present Godunov method with alternate methods available in the literature. One such method, discussed in [18], employs an HLL approximate Riemann solver to determine the conservative contribution to the numerical flux functions. The discretization of the non-conservative terms, on the other hand, is guided by the condition that constant velocity and pressure is maintained exactly in the numerical solution of free-streaming flow. Both first-order and second-order methods are described in [18], but we will focus on the simpler first-order method for purposes of comparison. The first-order method may be written in the form of (33), but with flux functions $\mathbf{F}_L$ and $\mathbf{F}_R$ given by

Table 4
Numerical errors and convergence rates for the first-order, G_1, and second-order, G_2, methods

N	G_1		G_2		G_2 (no limiter)	
	E_N	r_N	E_N	r_N	E_N	r_N
100	1.05×10^{-2}		1.12×10^{-4}		3.56×10^{-4}	
200	5.31×10^{-3}	0.98	3.14×10^{-4}	1.83	9.75×10^{-5}	1.87
400	2.75×10^{-3}	0.95	9.16×10^{-5}	1.78	1.71×10^{-5}	1.92
800	1.38×10^{-3}	1.00	2.72×10^{-5}	1.75	6.61×10^{-6}	1.97

$$\mathbf{F}_{\mathrm{L}}(\mathbf{U}^n_{j-1},\mathbf{U}^n_j)=\mathbf{F}_{\mathrm{HLL}}(\mathbf{U}^n_{j-1},\mathbf{U}^n_j)-\mathbf{h}(\mathbf{U}^n_{j-1})\left(\frac{\lambda_+\bar{\alpha}^n_{j-1}-\lambda_-\bar{\alpha}^n_j}{\lambda_+-\lambda_-}\right)$$

and

$$\mathbf{F}_{\mathrm{R}}(\mathbf{U}^n_{j-1},\mathbf{U}^n_j)=\mathbf{F}_{\mathrm{HLL}}(\mathbf{U}^n_{j-1},\mathbf{U}^n_j)-\mathbf{h}(\mathbf{U}^n_{j})\left(\frac{\lambda_+\bar{\alpha}^n_{j-1}-\lambda_-\bar{\alpha}^n_j}{\lambda_+-\lambda_-}\right),$$

where

$$\mathbf{F}_{\mathrm{HLL}}(\mathbf{U}^n_{j-1},\mathbf{U}^n_j)=\frac{\lambda_+\mathbf{f}(\mathbf{U}^n_{j-1})-\lambda_-\mathbf{f}(\mathbf{U}^n_j)+\lambda_+\lambda_-(\mathbf{U}^n_j-\mathbf{U}^n_{j-1})}{\lambda_+-\lambda_-}$$

has the form of the usual HLL flux function [27] with approximate wave speeds taken to be

$$\lambda_+=\max_{k=j-1,j}\{0,\bar{v}^n_k+\bar{a}^n_k,v^n_k+a^n_k\},\quad \lambda_-=\min_{k=j-1,j}\{0,\bar{v}^n_k-\bar{a}^n_k,v^n_k-a^n_k\}.$$

We shall refer to this method as G_{HLL}. Another method, described by Andrianov et al. [19], determines the conservative contribution to the numerical fluxes based on the exact solution of a linearized Riemann problem. The discretization of the non-conservative terms is guided again by a condition based on preserving free-streaming flow. A version of this method takes the form of (33), and uses flux functions

$$\mathbf{F}_{\mathrm{L}}(\mathbf{U}^n_{j-1},\mathbf{U}^n_j)=\begin{cases}\mathbf{f}(\mathbf{u}^*(\mathbf{U}^n_{j-1},\mathbf{U}^n_j))-\mathbf{h}(\mathbf{U}^n_{j-1})\bar{\alpha}^n_j & \text{if } \bar{v}^n_{c,j-1/2}<0,\\ \mathbf{f}(\mathbf{u}^*(\mathbf{U}^n_{j-1},\mathbf{U}^n_j))-\mathbf{h}(\mathbf{U}^n_{j-1})\bar{\alpha}^n_{j-1} & \text{if } \bar{v}^n_{c,j-1/2}>0,\end{cases}$$

and

$$\mathbf{F}_{\mathrm{R}}(\mathbf{U}^n_{j-1},\mathbf{U}^n_j)=\begin{cases}\mathbf{f}(\mathbf{u}^*(\mathbf{U}^n_{j-1},\mathbf{U}^n_j))-\mathbf{h}(\mathbf{U}^n_{j})\bar{\alpha}^n_j & \text{if } \bar{v}^n_{c,j-1/2}<0,\\ \mathbf{f}(\mathbf{u}^*(\mathbf{U}^n_{j-1},\mathbf{U}^n_j))-\mathbf{h}(\mathbf{U}^n_{j})\bar{\alpha}^n_{j-1} & \text{if } \bar{v}^n_{c,j-1/2}>0.\end{cases}$$

Here, we have replaced a linearized Godunov flux with the exact one given by $\mathbf{f}(\mathbf{u}^*(\mathbf{U}^n_{j-1},\mathbf{U}^n_j))$, but the numerical approximation of the non-conservative terms follows that described in [19]. This latter method will be referred to as G_{ASW}.

Fig. 16 provides a comparison of the numerical solutions given by the first-order methods G_{HLL}, G_{ASW} and G_1 of the Riemann problem with left and right states given in Table 1. Fig. 16(a) shows the behavior of $\bar{\alpha}$ versus x at $t=0.2$. Here, we note that both G_{ASW} and G_1 resolve the solid contact with minimal numerical dissipation while there is significantly more smearing seen in the solution given by G_{HLL}. A closer look at the behavior in the solid contact layer is shown, for example, in the plot $\bar{p}$ versus $\bar{\alpha}$ given in Fig. 16(b). In this plot, we see that the numerical solutions given by G_{HLL} and G_{ASW} differ from that given by the layer equations in (55). This is due to the numerical approximation of the non-conservative terms, which is guided by a free-streaming condition for both of these methods. While this condition is effective in many cases, it ignores the details of the layer and thus suffers from a loss of accuracy in others. The present method, G_1, on the other hand, is in better agreement with the layer solution. The effect of the disagreement through the solid contact layer may be seen in Figs. 16(c) and (d) where we plot numerical solutions for $\bar{\rho}$ and ρ, respectively, versus x. Aside from the significant smearing in the solution given by G_{HLL}, we note an error in the states on both sides of the solid contact as determined by G_{HLL} and G_{ASW}. The example shown in Fig. 16 provides an indication of the effect of the solid contact layer on the numerical solution, and the accuracy of the numerical approach presented in this paper. In general, we find that the present numerical approach shows similar accuracy in the layer for any solution configuration, and for cases with a large jump in the volume fraction through the layer it gives equal or better accuracy than the solutions given by G_{HLL} or G_{ASW} for all test cases we have considered.

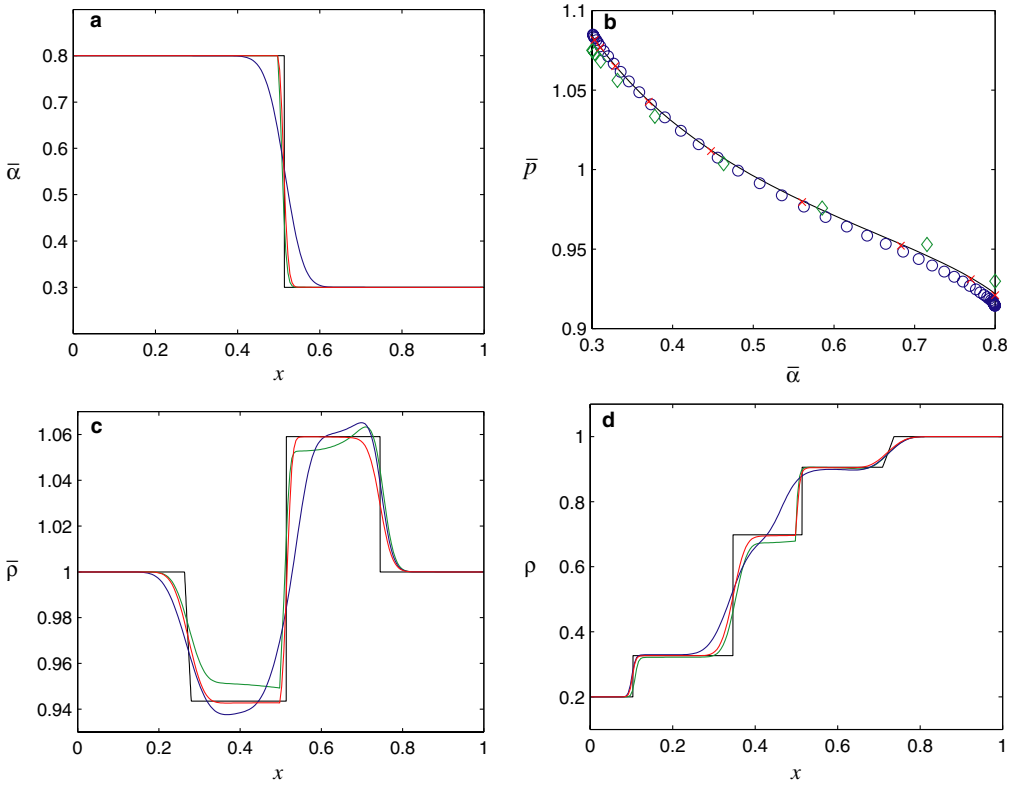

Fig. 16. Numerical solutions at $t = 0.2$ of the Riemann problem with left and right states given in Table 1. The curves and marks are given by methods G_{HLL} (blue), G_{ASW} (green) G_1 (red) all with 200 grid cells. The exact solution appears in black. (For interpretation of the references to color in this figure legend, the reader is referred to the web version of this article.)

8. Conclusions

We have considered the structure of the Riemann problem for the Baer and Nunziato equations modeling compressible two-phase flow (without exchange source terms). The solution consists of shocks, rarefactions and contact discontinuities in the various characteristic fields of the separate phases with the coupling between phases being confined to a (infinitesimally) thin region about the solid contact. In this thin region, the non-conservative terms in the governing equations contribute and are handled by assuming a quasi-steady thin layer approximation. An analysis of this thin layer results in nonlinear equations that determine the jump in the state across the solid contact. These jump conditions agree with those obtained by Embid and Baer [10] using generalized Riemann invariants. A two-stage iterative procedure has been described to solve the Riemann problem for given left and right states of the flow. This procedure makes no initial assumption regarding the wave structure of the flow, but rather computes it as part of the iterative solution procedure. The iterative procedure was used to compute solutions for a representative case in which the left and right states consist of a mixture of the phases, and for special cases in which one of the phases vanishes in the left or right states.

The exact solution for the Riemann problem was used to develop a Godunov method for the model equations. Here, we considered an integration of the governing equations over a grid cell and used the exact solution of the Riemann problem to evaluate both the integral of the conservative fluxes and the integral of

the non-conservative terms. The latter integration reduced to a contribution across the solid contact that forms from each cell boundary and was evaluated using the thin layer equations. The contribution from the non-conservative terms was combined with the conservative part of the fluxes to form a first-order approximation of the governing equations. The numerical method was shown to reduce to the standard Godunov method for the Euler equations in the special case when the phases decouple and was shown to maintain constant pressure and velocity exactly in the special case of free-streaming flow. An adaptive Riemann solver was presented and used to reduce the computational cost in the calculation of the combined fluxes and a second-order extension of the Godunov method was developed based on a slope-limiting approach.

Various numerical experiments were performed in order to study the behavior and assess the accuracy of the first-order and second-order methods. Numerical solutions of the model equations subject to piecewise constant initial data were shown to agree well with the corresponding exact solutions of the Riemann problem. Good agreement was obtained for cases in which the left and right states consisted of a mixture of the phases, and for cases in which one of the phases vanished in the flow. Of particular interest in these flows was the behavior of the numerical solution near the solid contact, where the phases couple and the non-conservative terms are important. A close study of the numerical results near the solid contact showed that both the first-order and second-order solutions agreed well with the behavior determined by the thin-layer equations. This suggests that the present numerical method accurately captures the assumed behavior and jump conditions across the solid contact layer.

Smooth solutions of the governing equations were considered and solved numerically in order to verify the order of accuracy of the first-order and second-order methods, and, finally, two other numerical methods of solution suggested by the work in [18,19] were compared with the present Godunov scheme. The former scheme employs an HLL approximate Riemann solver to evaluate the conservative contribution of the numerical fluxes while the latter scheme uses an exact solution of a linearized Riemann problem to determine the conservative portion of the flux, but this was replaced by an exact solution of the Riemann problem in our implementation of the method. Both schemes use a condition based on preserving free-streaming flow in order to discretize the non-conservative terms. A close study of these two methods for a problem involving a moderate jump in $\bar{\alpha}$ at the solid contact showed that the Godunov method developed here performed better through the solid contact layer which resulted in better agreement with the states of the solution on either side of the layer.

The numerical method considered here provides a useful foundation for further studies of the full model upon inclusion of the exchange source terms. In addition, the method may be extended to handle more general equations of state and problems in more space dimensions. These paths are under consideration for future research.

References

[1] M.R. Baer, J.W. Nunziato, A two-phase mixture theory for the deflagration-to-detonation transition (DDT) in reactive granular materials, Int. J. Multiphase Flow 12 (1986) 861–889.
[2] P.B. Butler, H. Krier, Analysis of deflagration-to-detonation transition in high-energy solid propellants, Combust. Flame 63 (1986) 31.
[3] S.S. Gokhale, H. Krier, Modeling of unsteady two-phase reactive flow in porous beds of propellants, Prog. Energy Combust. Sci. 8 (1982) 1.
[4] J.M. Powers, D.S. Stewart, H. Krier, Theory of two-phase detonation, Part I: Modeling, Combust. Flame 80 (1990) 264.
[5] J.M. Powers, D.S. Stewart, H. Krier, Theory of two-phase detonation, Part II: structure, Combust. Flame 80 (1990) 280.
[6] B.W. Asay, S.F. Son, J.B. Bdzil, The role of gas permeation in convective burning, Int. J. Multiphase Flow 23 (5) (1996) 923–952.
[7] S.K. Godunov, Difference methods for the numerical calculation of the equations of fluid dynamics, Mater. Sb. 47 (1959) 271–306.
[8] B. van Leer, Towards the ultimate conservative difference scheme, V. A second-order sequel to Godunov's method, J. Comput. Phys. 32 (1979) 101–136.

[9] J. Bell, P. Colella, J. Trangenstein, Higher order Godunov methods for general systems of hyperbolic conservation laws, J. Comput. Phys. 82 (1989) 362–397.
[10] P. Embid, M. Baer, Mathematical analysis of a two-phase continuum mixture theory, Continuum Mech. Thermodyn. 4 (1992) 279–312.
[11] A.K. Kapila, S.F. Son, J.B. Bdzil, R. Menikoff, D.S. Stewart, Two-phase modeling of DDT: structure of the velocity-relaxation zone, Phys. Fluids 9 (12) (1997) 3885–3897.
[12] J.B. Bdzil, R. Menikoff, S.F. Son, A.K. Kapila, D.S. Stewart, Two-phase modeling of deflagration-to-detonation transition in granular materials: a critical examination of modeling issues, Phys. Fluids 11 (2) (1999) 378–402.
[13] A.K. Kapila, R. Menikoff, J.B. Bdzil, S.F. Son, D.S. Stewart, Two-phase modeling of deflagration-to-detonation transition in granular materials: reduced equations, Phys. Fluids 13 (10) (2001) 3002–3024.
[14] J.B. Bdzil, S.F. Son, Engineering models of deflagration-to-detonation transition, LANL Report LA-12794-MS.
[15] N. Andrianov, G. Warnecke, The Riemann problem for the Baer–Nunziato two-phase flow model, J. Comput. Phys. 195 (2004) 434–464.
[16] K.A. Gonthier, J.M. Powers, A numerical investigation of transient detonation in granulated material, Shock Waves 6 (1996) 183–195.
[17] K.A. Gonthier, J.M. Powers, A high-resolution numerical method for a two-phase model of deflagration-to-detonation transition, J. Comput. Phys. 163 (2000) 376–433.
[18] R. Saurel, R. Abgrall, A multiphase Godunov method for compressible multifluid and multiphase flows, J. Comput. Phys. 150 (1999) 425–467.
[19] N. Andrianov, R. Saurel, G. Warnecke, A simple method for compressible multiphase mixtures and interfaces, Technical Report 4247, INRIA, 2001.
[20] R. Saurel, O. Lemetayer, A multiphase model for compressible flows with interfaces, shocks, detonation waves and cavitation, J. Fluid Mech. 431 (2001) 239–271.
[21] S. Gavrilyuk, R. Saurel, Mathematical and numerical modeling of two-phase compressible flows with micro-inertia, J. Comput. Phys. 175 (2002) 326–360.
[22] R. Abgrall, R. Saurel, Discrete equations for physical and numerical compressible multiphase mixtures, J. Comput. Phys. 186 (2003) 361–396.
[23] R. Abgrall, How to prevent pressure oscillations in mulicomponent flow calculations: a quasi conservative approach, J. Comput. Phys. 125 (1996) 150–160.
[24] E.F. Toro, Riemann Solvers and Numerical Methods for Fluid Dynamics, Springer, Berlin, 1999.
[25] R.J. LeVeque, Numerical Methods for Conservation Laws, Birkhäuser, Basel, 1992.
[26] J.M. Powers, Two-phase viscous modeling of compaction in granular explosives, Phys. Fluids 16 (8) (2004) 2975–2990.
[27] A. Harten, P.D. Lax, B. van Leer, On upstream differencing and Godunov type schemes for hyperbolic conservation laws, SIAM Rev. 25 (1983) 33–61.